The Journal of Chemical Physics

Discrete and Continuous Models of Probability Flux of Switching Dynamics: Uncovering Stochastic Oscillations in a Toggle-Switch System

Anna Terebus,[1] Chun Liu,[2] and Jie Liang[1, a)]
[1)] *Department of Bioengineering, University of Illinois at Chicago, Chicago IL, 60607, USA.*
[2)] *Department of Applied Mathematics, Illinois Institute of Technology, Chicago IL, 60616, USA*

Probability flux and velocity in stochastic reaction networks can help characterizing dynamic changes in probability landscapes of these networks. Here we study the behavior of three different models of probability flux, namely, the discrete flux model, the Fokker-Planck model, and a new continuum model of the Liouville flux. We compare these fluxes which are formulated based on, respectively, chemical master equation, stochastic differential equation, and ordinary differential equation. We examine similarities and differences among these models at the nonequilibrium steady state for the toggle switch network under different binding and unbinding conditions. Our results show that at strong stochastic condition of weak promoter binding, continuum models of Fokker-Planck and Liouville fluxes deviate significantly from the discrete flux model. Furthermore, we report the discovery of stochastic oscillation in the toggle-switch system occurring at weak binding conditions, a phenomenon only captured by the discrete flux model.

Keywords: Toggle-switch network, discrete flux and velocity fields of probability, Fokker-Planck flux, Liouville flux

Networks of chemical reactions can depict how interactions among molecules of DNA, RNA, and protein regulate gene expression. These networks, called gene regulatory networks, play important roles in biological processes such as cell fate determination[1,2], signal transduction[3,4], and metabolic regulations[5?] . When genes, transcription factors, signaling molecules, and regulatory proteins are in small quantities, stochasticity plays important roles[6–8]. Characterizing the probability surfaces of molecules of gene regulatory networks can help to understand their behavior.

The general stochastic process dictated by chemical reactions has two complementary representations, one in the form of reaction path or reaction trajectory, another in the form of time-evolving probability density function. The microstates of chemical reaction system are integer vectors of copy numbers of different types of molecules. Specifically, the Stochastic Chemical Kinetics (SCK) processes of reactions can be described either by trajectories of reaction paths, which follow a random-time changed integral equations of Poisson process[9,10], or by the time-evolving probability density function governed by the discrete Chemical Master Equation[11–13].

The Stochastic Simulation Algorithm (SSA) and related methods[10,14–17] can be used to generate trajectories of reaction paths following the random time changed Poisson integral equation. A number of methods has also been developed that can be used to compute the time-evolving probability density function[18–22]. Among these, the ACME method constructs an explicit state space optimally enumerated on a n-simplex and can be used to compute the time-evolving probability density function for a large number of networks, with truncation errors *a priori* bounded[21,22].

When the microstates of reaction system are approximated as vectors in continuous space, the corresponding continuous stochastic processes can be represented either by reaction trajectories following stochastic differential equations (SDEs) such as the chemical Langevin equation[15], or by time-evolving probability density governed by Fokker-Planck Equation[23–28].

Ordinary differential equations models, under further simplifying assumptions of large copy numbers in large volume, can describe changes in mean concentrations of the molecular species, although stochasticity is not taken into account[29,30].

Furthermore, it is also essential to characterize the probability flux in reaction systems for understanding the biochemistry of living things[23,24,31–36]. Probability flux and velocity field can help to infer the mechanisms of network functions such as switching between cellular states[31,32], and to identify barriers and checkpoints between cellular states[27]. Furthermore, flux and velocity fields of probability can characterize the departure of non-equilibrium steady state from equilibrium, aiding in understanding of the non-linear behavior of these networks[28,35,37]. Computing probability fluxes and velocity fields has also found applications in studies of stem cell differentiation[38], cell cycle[27], and cancer development[39,40].

Among early studies of probability fluxes, Hill examined reaction fluxes of discrete-state continuous-time Markov model, and introduced various forms of fluxes, including one-way transition flux, net flux, cycle fluxes, and operational flux[41]. This and many subsequent important studies are based on a view centered on reactions, where states correspond to specific nodes on diagrams of kinetic reactions, representing various forms of molecu-

[a)] Electronic mail: jliang@uic.edu.

lar species. We regard these models of fluxes as that of Lagrangian fluxes. An alternative view is to center on microstates in the state space, which are integer vectors of copy numbers. With this viewpoint, one examines fluxes resulting from firing of different chemical reactions, which flow into and out of individual fixed microstate. We regard such models of fluxes as Eulerian fluxes.

The universal discrete flux model based on Chemical Stochastic Kinetics was developed in a previous study for arbitrary stochstic networks of chemical reactions[36], with the Eulerian fluxes formulated based on discrete calculus defined for Chemical Stochastic Kinetics. Relationships between discrete Eulerian fluxes and reaction-based discrete Lagrangian fluxes were also given. This model enables the construction of global flow-maps of fluxes in all directions at every microstate, while satisfying the discrete version of the continuity equation. It can also be used to tag the probability fluxes of outflow and inflow as reactions proceeds[36].

While different models have been used to analyze gene regulatory networks, it is important to understand their applicability and limitations. For analysis of probability distribution of microstates, models based on ordinary differential equations generally are not applicable to stochastic systems, for example, those with low copy numbers of molecules or with large differences in reaction rates[30,42–44]. Models based on continuum approximations of the discrete Markov jump processes also have limitations: Fokker-Planck models may fail to capture the presence of multistability arising from slow switching between the ON and the OFF states[45]. Moreover, when systems are far from equilibrium, the probability landscape constructed using models based on continuum approximations is also of inadequate accuracy[46]. In general, the applicability and validity of these models for a specific network needs to be investigated individually[13,30,43–49].

Assessing the applicability and limitations of different models in the analysis of probability flux and velocity is more challenging. In this work, we study the applicability and the limitations of three classes of flux models. The first is the universal discrete flux models based on the original Stochastic Chemical Kinetic model[36]. This model overcome limitations in previous discrete models of probability flux and velocity in[31,50–53], such as restrictions to analysis of single reactional trajectories[50,51], to partial flux functions[31,52], or to single-species reactions[53].

Our second class of models are diffusion approximations of the Stochastic Chemical Kinetics, which can be represented either by the Chemical Langevin Equation for its stochastic trajectories[15], or by the Fokker-Planck equation for its time-evolving probability density[23–28]. The Fokker-Planck model we study are derived from the Kramers-Moyal expansion of the discrete Chemical Master Equation following reference[23]. Our third class of models is a novel probability flux model called the Liouville flux model that is the deterministic limit of the stochastic stochastic kinetic models. It is based on chemical rate equations and ordinary differential equations (ODEs). Although deterministic models of flux based on ODEs are generally not applicable to gene regulatory networks, the Liouville flux model treats the probability flux with precomputed probability distribution at individual states. It can be directly compared with the universal discrete flux and Fokker-Planck flux.

We examine the behavior of the probability fluxes using the toggle switch system. We study the steady state fluxes under two conditions, i) when the binding rates of the transcription factors to promoters of genes are much higher than the unbinding rates, under which the system exhibiting three stable states, and ii) when the unbinding rates are of the same magnitude as binding rates, under which the system is strongly stochastic and exhibits four stable states. Our results show that fluxes computed with these three different models all have similar behavior under the first condition, but exhibit markedly different behaviors under the second condition. Furthermore, we show that the universal discrete stochastic flux can uncover oscillating behavior of the toggle switch system at the non-equilibrium steady state, while Fokker-Planck and Liouville models fail to capture this highly stochastic phenomenon.

Our paper is organized as follows. We first introduce the three flux models and give closed-forms of the differences among these models. We then examine details of the differences in probability fluxes in the toggle switch network under the two conditions.

I. MODELS AND METHODS

A. Model of Biochemical Reactions Networks

We consider a well-mixed system of reactions with constant volume and temperature. It has n molecular species X_i, $i = 1, \ldots, n$, which participate in m reactions R_k, $k = 1, \ldots, m$. The *microstate* $\mathbf{x}(t)$ of the system at time t is a column vector of copy numbers of the molecular species: $\mathbf{x}(t) \equiv (x_1(t), x_2(t), \ldots, x_n(t))^T \in \mathbb{Z}_+^n$, where all values are non-negative integers. *A reaction* R_k takes the general form of

$$R_k : c_{1_k} X_1 + \cdots + c_{n_k} X_n \xrightarrow{r_k} c'_{1_k} X_1 + \cdots + c'_{n_k} X_n,$$

so that R_k brings the system from a microstate $\mathbf{x}$ to $\mathbf{x} + \mathbf{s}_k$, where the stoichiometry vector $\mathbf{s}_k$ is defined as:

$$\mathbf{s}_k \equiv (s_k^1, \ldots, s_k^n) \equiv (c'_{1_k} - c_{1_k}, \ldots, c'_{n_k} - c_{n_k}), \qquad (1)$$

which gives the unit vector of *the discrete increment* of reaction R_k. $\mathbf{s}_k$ also defines *the direction of* R_k.

B. Discrete Chemical Master Equation (dCME)

The discrete Chemical Master Equation (dCME) consists of a set of linear ordinary differential equations de-

scribing the changes of probability over time at each microstate of a reaction system[2,10,19,54]. Denote the probability of the system to be at a particular microstate $\mathbf{x}$ at time t as $p(\mathbf{x},t) \in \mathbb{R}_{[0,1]}$. Denote the probability surface or landscape over the state space Ω as $\mathbf{p}(t) = \{p(\mathbf{x}(t)|\mathbf{x}(t) \in \Omega)\}$. The dCME at an arbitrary microstate $\mathbf{x} = \mathbf{x}(t)$ can be written in the general form as:

$$\frac{\partial p(\mathbf{x},t)}{\partial t} = \sum_{k=1}^{m} [A_k(\mathbf{x}-\mathbf{s}_k)p(\mathbf{x}-\mathbf{s}_k,t) - A_k(\mathbf{x})p(\mathbf{x},t)], \tag{2}$$

$\mathbf{x}-\mathbf{s}_k, \mathbf{x} \in \Omega$. Here the reaction propensity $A_k(\mathbf{x})$ is determined by the product of the intrinsic reaction rate r_k and the combinations of copies of relevant reactants at the current microstate $\mathbf{x}$: $A_k(\mathbf{x}) = r_k \prod_{l=1}^{n} \begin{pmatrix} x_l \\ c_{lk} \end{pmatrix}$.

For computing the probability distribution, we employ the recently developed ACME method[21,22] to solve the dCME underlying the stochastic network and obtain its exact time-evolving probability surfaces.This eliminates potential problems arising from inadequate sampling, where rare events of low probability are difficult to quantify using techniques such as the stochastic simulations algorithm (SSA)[10,16,17,55].

C. Continuum Approximations of dCME

1. Deterministic Equation from Law of Mass Action

Deterministic model of reactions describes the time-evolving mean value or concentration $\langle X_i \rangle$ of each molecular species X_i. The ordinary differential equations can be written generically at $\langle \mathbf{X} \rangle = (\langle X_1 \rangle, \ldots, \langle X_n \rangle)$ as

$$\frac{d\langle \mathbf{X} \rangle}{dt} = \mathbf{F}(\langle \mathbf{X} \rangle). \tag{3}$$

Here the functions

$$\begin{aligned} \mathbf{F}(\langle \mathbf{X} \rangle) \equiv & (F_1(\langle X_1 \rangle, \ldots, \langle X_n \rangle), \\ & \ldots, F_n(\langle X_1 \rangle, \ldots, \langle X_n \rangle)) \end{aligned} \tag{4}$$

characterize how the the *vector of molecular concentrations* $\langle \mathbf{X} \rangle$ changes with time.

A standard approach for such a characterization is based on chemical rate equations[56]. Here the rate of a chemical reaction is directly proportional to the product of the activities or concentrations of the reactants. Therefore, functions $F_i(\langle \mathbf{X} \rangle)$ in Eqn.(4) can be written, as:

$$F_i(\langle \mathbf{X} \rangle) = \sum_{k=1}^{m} \mathrm{sgn}(s_k^i) r_k \langle X_1 \rangle^{|c_{1_k}|} \cdot \ldots \cdot \langle X_n \rangle^{|c_{n_k}|}, \tag{5}$$

where s_k^i are the components of stoichiometry vector $\mathbf{s}_k$ and r_k the intrinsic reaction rate of reaction R_k.

The Law of Mass Action can be derived from dCME (Eqn. (2)) using the theory of moment-closure approximations at high copy numbers[42,57–59].

2. Approximation Model of Fokker-Planck Equation

The continuous diffusion approximation in the form of a Fokker-Planck model can be derived from the discrete Chemical Master Equation under the assumptions of i) small jumps between states due to firing of reactions, namely, $|s_k/V| < \epsilon$, where $\epsilon \to 0$, ii) slow changes of the probability, namely, $|p(x) - p(x+s_k/V)| < \delta$ where $\delta \to 0$ for reaction R_k, whose stoichiometry is s_k and the system volume is V. With these assumptions, the transition kernel $A_k(\mathbf{x}-\mathbf{s}_k/V)p(\mathbf{x}-\mathbf{s}_k/V,t)$ is differentiable to a high degree.

The model of the Fokker-Planck equation considered in this work is derived from the multivariate Taylor expansion or the Kramers-Moyal expansion of the dCME[23]:

$$\begin{aligned} \frac{\partial p(\mathbf{x},t)}{\partial t} &= \sum_{k=1}^{m} [A_k(\mathbf{x}-\frac{\mathbf{s}_k}{V})p(\mathbf{x}-\frac{\mathbf{s}_k}{V},t) - A_k(\mathbf{x})p(\mathbf{x},t)] \\ &\approx \sum_{k=1}^{m} [A_k(\mathbf{x})p(\mathbf{x},t) - \frac{\mathbf{s}_k}{V}\nabla_{\mathbf{x}} A_k(\mathbf{x})p(\mathbf{x},t) \\ &\quad + \frac{\mathbf{s}_k \cdot \mathbf{s}_k^T}{2V^2}\nabla_{\mathbf{x}}^2 A_k(\mathbf{x})p(\mathbf{x},t) - A_k(\mathbf{x})p(\mathbf{x},t)] \\ &= \sum_{k=1}^{m} [-\frac{\mathbf{s}_k}{V}\nabla_{\mathbf{x}} A_k(\mathbf{x})p(\mathbf{x},t) \\ &\quad + \frac{\mathbf{s}_k \cdot \mathbf{s}_k^T}{2V^2}\nabla_{\mathbf{x}}^2 A_k(\mathbf{x})p(\mathbf{x},t)]. \end{aligned} \tag{6}$$

In Fokker-Planck models, terms higher than two are neglected[23].

D. Continuity Equation of Probability.

The evolution of the probability landscape can be viewed as a process of movement of probability mass in the state space. The total probability mass is conserved at any time and sums up to one. This is captured by the continuity equation for probability[60,61]. It is defined on a set of average molecular mass concentrations $\langle \mathbf{X} \rangle = (\langle X_1 \rangle, \ldots, \langle X_n \rangle) \in \mathbb{R}_+^n$:

$$\frac{\partial p(\langle \mathbf{X} \rangle, t)}{\partial t} + \nabla_{\langle \mathbf{X} \rangle} \mathbf{J}(\langle \mathbf{X} \rangle, t) = 0, \tag{7}$$

which defines $\mathbf{J}(\langle \mathbf{X} \rangle, t)$, the vector of probability flux, namely, the flow of probability in the direction of each species.

As the velocity of the probability is related to the flux by the relationship $\mathbf{v}(\langle \mathbf{X} \rangle, t) = \mathbf{J}(\langle \mathbf{X} \rangle, t)/p(\langle \mathbf{X} \rangle, t)$, the

continuity equation can also be written for velocity as:

$$\frac{\partial p(\langle \mathbf{X} \rangle, t)}{\partial t} + \nabla_{\langle \mathbf{X} \rangle} \mathbf{v}(\langle \mathbf{X} \rangle, t) p(\langle \mathbf{X} \rangle, t) = 0. \tag{8}$$

Similar to Eqn.(7), a discrete version of the continuity equation,

$$\frac{\partial p(\mathbf{x}, t)}{\partial t} + \nabla_d \cdot \mathbf{J}_r(\mathbf{x}, t) = 0, \tag{9}$$

holds for the total reactional flux defined in[36].

E. Models of Probability Flux

1. Liouville Flux Model

Here we introduce a Liouville flux model based on the ordinary differential equations for mean concentrations of molecules from mass action. It is a set of forward differential equation, in which the increment in the mean concentration of molecular specie over time $\partial\langle \mathbf{X} \rangle / \partial t$, given $\partial t \to 0$, defines the Liouville velocity $\mathbf{v}_L(\langle \mathbf{X} \rangle, t)$ of reactional mass of the average molecular concentration $\langle \mathbf{X} \rangle$:

$$\mathbf{v}_L(\langle \mathbf{X} \rangle, t) = \mathbf{F}(\langle \mathbf{X} \rangle, t),$$

where the components of $\mathbf{F}(\langle \mathbf{X} \rangle, t)$ are defined by Eqn.(5).

To compare with other flux models, we now restrict the values of the function $\mathbf{v}_L = \mathbf{v}_L(\langle \mathbf{X} \rangle, t)$ to the discrete state space Ω, where the probability values are computed using the ACME method[21,22]. We use the notation $\mathbf{v}_L \equiv \mathbf{v}_L(\mathbf{x}, t)$.

The Liouville flux is defined in the discrete subset Ω of the continuous space U as:

$$\mathbf{J}_L(\mathbf{x}, t) \equiv \mathbf{v}_L(\mathbf{x}, t) p(\mathbf{x}, t). \tag{10}$$

2. Fokker-Planck Flux Model

We rewrite the right hand side of Eqn.(6) by taking the operator $\nabla_{\mathbf{x}}(\cdot)$ outside the parenthesis:

$$\frac{\partial p(\mathbf{x}, t)}{\partial t} = -\nabla_{\mathbf{x}} \sum_{k=1}^{m} \frac{\mathbf{s}_k}{V} [A_k(\mathbf{x}) p(\mathbf{x}, t) - \frac{\mathbf{s}_k{}^T}{2V} \nabla_{\mathbf{x}} A_k(\mathbf{x}) p(\mathbf{x}, t)].$$

From Eqn.(7), the flux for the Fokker-Planck model $\mathbf{J}_{FP}(\mathbf{x}, t)$ can be written as follows:

$$\mathbf{J}_{FP}(\mathbf{x}, t) \equiv \sum_{k=1}^{m} \frac{\mathbf{s}_k}{V} [A_k(\mathbf{x}) p(\mathbf{x}, t) - \frac{\mathbf{s}_k{}^T}{2V} \nabla_{\mathbf{x}} A_k(\mathbf{x}) p(\mathbf{x}, t)]. \tag{11}$$

The Fokker-Plank flux Eqn.(11) has two components: the drift term of $\sum_{k=1}^{m} \mathbf{s}_k A_k(\mathbf{x}) p(\mathbf{x}, t)/V$ and the diffusion term of $\sum_{k=1}^{m} \mathbf{s}_k \mathbf{s}_k^T \nabla_{\mathbf{x}} A_k(\mathbf{x}) p(\mathbf{x}, t)/(2V^2)$. The drift term is driven by chemical reactions occurring at $\mathbf{x}$. The diffusion term approximates linearly the stochastic fluctuations of the system.

3. Universal Discrete Flux Model

A model of discrete flux was recently introduced in reference[36]. As it can account for both reactional flux and species flux, we call it *the universal discrete flux model*. Briefly, we define an unambiguous order of ascending relationship " $\prec''$ over all microstates, and have them ordered as $\mathbf{x}^0 \prec \mathbf{x}^1 \prec \ldots \prec \mathbf{x}^{|\Omega|}$[36]. The *single-reactional flux of probability* $J_k(\mathbf{x}, t) \in \mathbb{R}$ for reaction R_k is:

$$J_k(\mathbf{x}, t) \equiv \begin{cases} A_k(\mathbf{x}) p(\mathbf{x}, t), & \mathbf{x} \prec \mathbf{x} + \mathbf{s}_k, \\ A_k(\mathbf{x} - \mathbf{s}_k) p(\mathbf{x} - \mathbf{s}_k, t), & \mathbf{x} \prec \mathbf{x} - \mathbf{s}_k. \end{cases}$$

$J_k(\mathbf{x}, t)$ depicts the change in $p(\mathbf{x}, t)$ at the state $\mathbf{x}$ due to one firing of reaction R_k. If $\mathbf{x} \prec \mathbf{x} + \mathbf{s}_k$, $J_k(\mathbf{x}, t)$ describes the outflux at $\mathbf{x}$ due to one firing of reaction R_k. If $\mathbf{x} \prec \mathbf{x} - \mathbf{s}_k$, $J_k(\mathbf{x}, t)$ describes the influx to $\mathbf{x}$ due to one firing of reaction R_k.

The *total reactional flux* or *r-flux* $\mathbf{J}_r(\mathbf{x}, t)$, which describes the probability flux at a microstate $\mathbf{x}$ at time t, is defined as[36]: $\mathbf{J}_r(\mathbf{x}, t) \equiv (J_1(\mathbf{x}, t), \cdots, J_m(\mathbf{x}, t)) \in \mathbb{R}^m$. Intuitively, the r-flux $\mathbf{J}_r(\mathbf{x}, t)$ is the vector of rate change of the probability mass at $\mathbf{x}$ in directions of all reactions. $J_r(\mathbf{x}, t)$ satisfies the discrete continuity equation Eqn. (9). Details can be found in[36].

The *total species flux*, or *s-flux*, $\mathbf{J}_s(\mathbf{x}, t) \in \mathbb{R}^n$ is the sum of the stoichiometry projections of m single-reaction species flux vectors at a microstate $\mathbf{x} \in \mathbb{R}^n$:

$$\mathbf{J}_s(\mathbf{x}, t) = \sum_{\mathrm{k}\,=\,1}^{\mathrm{m}} \mathbf{s}_k J_k(\mathbf{x}, t) \in \mathbb{R}^n. \tag{12}$$

F. Differences between flux models

We now compare the three flux models and define analytically their differences.

1. Difference between Discrete Flux and Fokker-Planck Flux

The difference between the universal discrete flux of Eqn. (12) and the Fokker-Planck flux of Eqn. (11) at

$V = 1$ is:

$$\begin{aligned}
&\mathbf{J}_s(\mathbf{x},t) - \mathbf{J}_{FP}(\mathbf{x},t) \\
&\quad = \sum_{\substack{k:\,\mathbf{x}\prec \\ \mathbf{x}+\mathbf{s}_k}} \mathbf{s}_k[A_k(\mathbf{x})p(\mathbf{x},t) - A_k(\mathbf{x})p(\mathbf{x},t) \\
&\qquad\qquad + \frac{\mathbf{s}_k}{2}\nabla_{\mathbf{x}}A_k(\mathbf{x})p(\mathbf{x},t)] \\
&\qquad + \sum_{\substack{k:\,\mathbf{x}\prec \\ \mathbf{x}-\mathbf{s}_k}} [\mathbf{s}_k A_k(\mathbf{x}-\mathbf{s}_k)p(\mathbf{x}-\mathbf{s}_k,t) \\
&\qquad\qquad - A_k(\mathbf{x})p(\mathbf{x},t) + \frac{\mathbf{s}_k}{2}\nabla_{\mathbf{x}}A_k(\mathbf{x})p(\mathbf{x},t)] \\
&\quad = \sum_{\substack{k:\,\mathbf{x}\prec \\ \mathbf{x}+\mathbf{s}_k}} \mathbf{s}_k\left[\frac{1}{2}\mathbf{s}_k\nabla_{\mathbf{x}}A_k(\mathbf{x})p(\mathbf{x},t)\right] \\
&\qquad + \sum_{\substack{k:\,\mathbf{x}\prec \\ \mathbf{x}-\mathbf{s}_k}} \mathbf{s}_k\left[A_k(\mathbf{x}-\mathbf{s}_k)p(\mathbf{x}-\mathbf{s}_k,t)\right. \\
&\qquad\qquad \left. - A_k(\mathbf{x})p(\mathbf{x},t) + \frac{\mathbf{s}_k}{2}\nabla_{\mathbf{x}}A_k(\mathbf{x})p(\mathbf{x},t)\right].
\end{aligned} \tag{13}$$

For reactions generating discrete flux out-flowing from $\mathbf{x}$ to $\mathbf{x}+\mathbf{s}_k$, the values of the discrete flux and Fokker-Planck flux differ only in the diffusion term $\mathbf{s}_k\left[\mathbf{s}_k\nabla_{\mathbf{x}}A_k(\mathbf{x})p(\mathbf{x},t)\right]/2$ of the Fokker-Planck flux. For reactions generating flux flowing-in from $\mathbf{x}-\mathbf{s}_k$ to $\mathbf{x}$, the discrete flux and Fokker-Planck flux differs in both the diffusion term and the drift term.

We examine the difference further by taking the linear Taylor expansion: $A_k(\mathbf{x}-\mathbf{s}_k)p(\mathbf{x}-\mathbf{s}_k,t) \approx A_k(\mathbf{x})p(\mathbf{x},t) - \mathbf{s}_k\nabla_{\mathbf{x}}A_k(\mathbf{x})p(\mathbf{x},t)$. While the gradient of the flux defines the change of the probability with time from the continuity equation, we now skip the second-order term of the Taylor expansion. Eqn. (13) now becomes:

$$\begin{aligned}
&\mathbf{J}_s(\mathbf{x},t) - \mathbf{J}_{FP}(\mathbf{x},t) \\
&\quad = \sum_{\substack{k:\,\mathbf{x}\prec \\ \mathbf{x}+\mathbf{s}_k}} \mathbf{s}_k\left[\frac{1}{2}\mathbf{s}_k\nabla_{\mathbf{x}}A_k(\mathbf{x})p(\mathbf{x},t)\right] \\
&\qquad + \sum_{\substack{k:\,\mathbf{x}\prec \\ \mathbf{x}-\mathbf{s}_k}} \mathbf{s}_k\left[A_k(\mathbf{x})p(\mathbf{x},t) - \mathbf{s}_k\nabla_{\mathbf{x}}A_k(\mathbf{x})p(\mathbf{x},t)\right. \\
&\qquad\qquad \left. -A_k(\mathbf{x})p(\mathbf{x},t) + \frac{1}{2}\mathbf{s}_k\nabla_{\mathbf{x}}A_k(\mathbf{x})p(\mathbf{x},t)\right] \\
&\quad = \sum_{\substack{k:\,\mathbf{x}\prec \\ \mathbf{x}+\mathbf{s}_k}} \mathbf{s}_k\left[\frac{1}{2}\mathbf{s}_k\nabla_{\mathbf{x}}A_k(\mathbf{x})p(\mathbf{x},t)\right] \\
&\qquad - \sum_{\substack{k:\,\mathbf{x}\prec \\ \mathbf{x}-\mathbf{s}_k}} \mathbf{s}_k\left[\frac{1}{2}\mathbf{s}_k\nabla_{\mathbf{x}}A_k(\mathbf{x})p(\mathbf{x},t)\right].
\end{aligned}$$

Hence, the drift terms for both fluxes are the same and equal to $A_k(\mathbf{x})p(\mathbf{x},t)$. The difference in these two flux models resides only in the noise encoded by the diffusion term.

2. Difference between Liouville Flux and Fokker-Planck Flux

The difference between the Fokker-Planck flux from Eqn. (11) and the Liouville flux from Eqn. (10), given $V = 1$, is:

$$\begin{aligned}
\mathbf{J}_{FP}(\mathbf{x},t) - \mathbf{J}_L(\mathbf{x},t) = \sum_k [&\mathbf{s}_k(A_k(\mathbf{x})p(\mathbf{x},t) \\
&- \frac{1}{2}\mathbf{s}_k\nabla_{\mathbf{x}}A_k(\mathbf{x})p(\mathbf{x},t))] - \mathbf{F}(\mathbf{x},t)p(\mathbf{x},t).
\end{aligned} \tag{14}$$

In this case, difference exists in both the drift term and the diffusion terms.

However, for the special case when there is only one type of reactant and $|\mathbf{s}_k| = 1$, we have $\mathbf{F}(\mathbf{x},t)p(\mathbf{x},t) = \mathbf{s}_k A_k(\mathbf{x})p(\mathbf{x},t)$. In this case, the drift terms of the two fluxes are the same.

Moreover in the limiting case of large concentrations, we have $\mathbf{F}(\mathbf{x},t) = \sum_k^m \mathbf{s}_k A_k(\mathbf{x})p(\mathbf{x},t)$. Therefore, the difference between Fokker-Planck flux and Liouville flux is only in diffusion term, which is generally of the order of $\frac{1}{2V}$.

3. Difference between Discrete Flux and Liouville Flux

The difference between the discrete universal flux (Eqn. (12)) and the Liouville flux (Eqn. (10)) is:

$$\begin{aligned}
&\mathbf{J}_s(\mathbf{x},t) - \mathbf{J}_L(\mathbf{x},t) = \\
&\qquad \sum_{\substack{k:\,\mathbf{x}\prec \\ \mathbf{x}+\mathbf{s}_k}} [\mathbf{s}_k A_k(\mathbf{x})p(\mathbf{x},t) - \mathbf{F}(\mathbf{x},t)p(\mathbf{x},t)] \\
&\quad + \sum_{\substack{k:\,\mathbf{x}\prec \\ \mathbf{x}-\mathbf{s}_k}} [\mathbf{s}_k A_k(\mathbf{x}-\mathbf{s}_k)p(\mathbf{x}-\mathbf{s}_k,t) - \mathbf{F}(\mathbf{x},t)p(\mathbf{x},t)].
\end{aligned} \tag{15}$$

We consider the special case of reactions involving only a single molecules species of reactants with $|\mathbf{s}_k| = 1$. We have $\mathbf{F}(\mathbf{x},t)p(\mathbf{x},t) = \mathbf{s}_k A_k(\mathbf{x})p(\mathbf{x},t)$. For reactions with probability flux flowing from $\mathbf{x}$ to $\mathbf{x}+\mathbf{s}_k$ ($\mathbf{x}-\mathbf{s}_k \prec \mathbf{x}$) both fluxes are the same. For reactions with probability flux flowing from $\mathbf{x}-\mathbf{s}_k$ to $\mathbf{x}$, we can examine this difference by taking the linear terms of the Taylor expansion of $A_k(\mathbf{x}-\mathbf{s}_k)p(\mathbf{x}-\mathbf{s}_k,t) \approx A_k(\mathbf{x})p(\mathbf{x},t) - \mathbf{s}_k\nabla_{\mathbf{x}}A_k(\mathbf{x})p(\mathbf{x},t)$. Eqn. (15) now becomes:

$$\begin{aligned}
&\mathbf{J}_s(\mathbf{x},t) - \mathbf{J}_L(\mathbf{x},t) \\
&\quad = \sum_{\substack{k:\,\mathbf{x}\prec \\ \mathbf{x}-\mathbf{s}_k}} [\mathbf{s}_k A_k(\mathbf{x}-\mathbf{s}_k)p(\mathbf{x}-\mathbf{s}_k,t) - \mathbf{F}(\mathbf{x},t)p(\mathbf{x},t)] \\
&\quad = \sum_{\substack{k:\,\mathbf{x}\prec \\ \mathbf{x}-\mathbf{s}_k}} [\mathbf{s}_k(A_k(\mathbf{x})p(\mathbf{x},t) - \mathbf{s}_k\nabla_{\mathbf{x}}A_k(\mathbf{x})p(\mathbf{x},t) \\
&\qquad\qquad - \mathbf{F}(\mathbf{x},t)p(\mathbf{x},t)].
\end{aligned}$$

In this case, under the assuption $\mathbf{F}(\mathbf{x},t)p(\mathbf{x},t) = \mathbf{s}_k A_k(\mathbf{x})p(\mathbf{x},t)$, the drift terms are the same. The fluxes differ only in the diffusion term $\mathbf{s}_k \nabla_{\mathbf{x}} A_k(\mathbf{x})p(\mathbf{x},t)$.

II. RESULTS

A. The Multistable Toggle Switch Model

1. Network and reactions

The toggle switch network consists of two genes whose protein products mutually inhibit each other. This network plays important roles in molecular decision-making and is widely found in nature[62–66]. Toggle switch has been studied extensively, with its stability, dynamics, switching mechanisms, and most-probable paths analyzed through outlfow probability fluxes[31], quasi-potential landscapes reconstruction[67], as well as weighted-ensemble trajectory simulations using the string-method[32]. In this study, we employ a detailed model of toggle switch[19,68], where the binding and unbinding reactions are explicitly modeled. This is different from the simplified model used in several other studies[62,69,70].

There are six molecular species in our model: genes G_x and G_y, which express proteins P_X and P_Y, as well as protein-DNA complexes $\overline{G}_x$ and $\overline{G}_y$, with protein P_Y bound on gene G_x and protein P_X bound on gene G_y, respectively (Figure 1). The dimer of protein product P_X of gene G_x inhibits the activity of gene G_y and the dimer of protein product P_Y of gene G_y inhibits the activity of gene G_x.

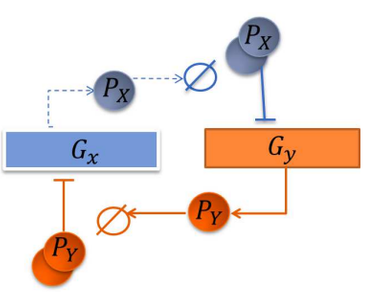

FIG. 1. Schematic representation of the toggle switch genetic network.

The molecular reactions of the network are listed below:

$$\begin{aligned}
&R_1 : G_x \xrightarrow{s_X} G_x + P_X, && R_2 : G_y \xrightarrow{s_Y} G_y + P_Y,\\
&R_3 : P_X \xrightarrow{d_X} \emptyset, && R_4 : P_Y \xrightarrow{d_Y} \emptyset,\\
&R_5 : 2P_X + G_y \xrightarrow{b_y} \overline{G}_y, && R_6 : 2P_Y + G_x \xrightarrow{b_x} \overline{G}_x,\\
&R_7 : \overline{G}_y \xrightarrow{u_y} 2P_X + G_y, && R_8 : \overline{G}_x \xrightarrow{u_x} 2P_Y + G_x.
\end{aligned} \tag{16}$$

The microstate of the system is defined as an ordered quadruplet (X, Y, x, y) of copy numbers of P_X, P_Y, G_x, and G_y, respectively. The copy numbers of bound genes $\overline{G}_x$ and $\overline{G}_y$ are denoted as $\overline{x}$ and $\overline{y}$. Correspondingly, $x = 1-\overline{x}$ and $y = 1-\overline{y}$, as there is only one copy of each of genes x and y in this system. The binding states of the two operator sites are denoted as "On-On" when $x = 1$ and $y = 1$, "On-Off" when $x = 1$ and $y = 0$, "Off-On" when $x = 0$ and $y = 1$, and "Off-Off", when $x = 0$ and $y = 0$.

There are a number of stochastic processes encoded in this network. The synthesis of proteins P_X and P_Y from gene G_x and gene G_y are represented by reactions R_1 and R_2, respectively, with the rates of $s_x = s_y$. The degradation of proteins P_X and P_Y are represented by reactions R_3 and R_4, respectively, with the rates $d_x = d_y$. Reaction R_5 represents the binding of two copies of protein P_X to the promoter site of G_y to form a protein-DNA complex $\overline{G}_y$, with rate b_y. Reaction R_7 represents the unbinding of the complex $\overline{G}_y$, at a rate of u_y. Similarly, reaction R_6 represents the binding of two copies of protein P_Y to the promoter site of G_x to form a protein-DNA complex $\overline{G}_x$, with rate b_x. Reaction R_8 represents the unbinding of the complex $\overline{G}_x$ at a rate of u_x.

Here we consider the scenario where gene regulation is much slower than protein synthesis and degradation. In eukaryotic cells, epigenetics processes such as histone modification and DNA methylation can reduce the binding rates of transcription factors to their targeting DNA sites. Recent findings in the genetic switch of bacteriophage λ showed that slower binding and unbinding also occur in bacterials cells[71]. In the regime of slow binding and unbinding reactions, where b_y and b_x (reactions R_5 and R_6) and u_y and u_x (reactions R_7 and R_8) are smaller than synthesis rates s_x and s_y (reactions R_1 and R_2), there are up to four peaks of probability over certain regions of protein copy numbers, in which one of the two genes is expressed and the other gene repressed, as well as two genes being either expressed or repressed simultaneously, as reported in[19].

A well-known phenomenon in genetic switches such as the toggle switch system is the extreme stability of the "On-Off" or the "Off-On" states: it is exceedingly rare for the system to switch from one of these two stable states to the other, even in the presence of perturbations[66,72]. In this study, we show that the toggle switch can switch frequently between these two stable states without external perturbations. Further, these switching events can turn the toggle switch into an stochastically oscillating system.

2. Fluxes in the Toggle Switch Network

For the universal discrete flux, we first impose an ascending order on the microstates in the direction of the increasing copies of X. At a fixed value of X, we then order the states in increasing copy number of Y. Subsequently, we order the states in increasing copy number

of x, and lastly, in the order of increasing copy number of y. Following Eqn. (12), components of the universal discrete stochastic fluxes at the microstate (X, Y, x, y) in the directions of X and Y are:

$$\begin{aligned} J_s(X,Y,x,y)_X &= s_X x p(X,Y,x,y) \\ &\quad - d_X(X+1)p(X+1,Y,x,y) \\ &\quad + 2u_y(1-y)p(X,Y,x,y) \\ &\quad - b_y(1-y)(X+1)(X+2)p(X+2,Y,x,1-y), \end{aligned}$$

$$\begin{aligned} J_s(X,Y,x,y)_Y &= s_Y y p(X,Y,x,y) \\ &\quad - d_Y(Y+1)p(X,Y+1,x,y) \\ &\quad + 2u_x(1-x)p(X,Y,x,y) \\ &\quad - b_x(1-x)(Y+1)(Y+2)p(X,Y+2,1-x,y). \end{aligned}$$

Following Eqn. (10), the Liouville flux at the microstate (X, Y, x, y) is:

$$\begin{aligned} J_L(X,Y,x,y)_X &= p(X,Y,x,y) \\ &\quad \times (s_X x - d_x X + u_y(1-y) - b_y X^2 y), \end{aligned}$$

$$\begin{aligned} J_L(X,Y,x,y)_Y &= p(X,Y,x,y) \\ &\quad \times (s_Y y - d_y Y + u_x(1-x) - b_x Y^2 x). \end{aligned}$$

Following Eqn. (11), the Fokker-Planck flux for $V = 1$ at the microstate (X, Y, x, y) is:

$$\begin{aligned} J_{FP}(X,Y,x,y)_X &= s_X x - d_X X + 2u_y(1-y) \\ &\quad - b_y X(X-1)y)p(X,Y,x,y) \\ &\quad + \frac{1}{2}\nabla_X[s_X x + d_X X + 2u_y(1-y) \\ &\quad + 2b_y X(X-1)y)p(X,Y,x,y)], \end{aligned}$$

$$\begin{aligned} J_{FP}(X,Y,x,y)_Y &= s_Y y - d_Y Y + 2u_x(1-x) \\ &\quad - b_x Y(Y-1)x)p(X,Y,x,y) \\ &\quad + \frac{1}{2}\nabla_Y[s_Y y + d_Y Y + 2u_x(1-x) \\ &\quad + 2b_x Y(Y-1)x)p(X,Y,x,y)]. \end{aligned}$$

B. Probability flux and velocity in toggle switch with strong promoter binding

We first consider the system with strong promoter binding. The binding rates are set to $b_x = b_y = 1 \times 10^{-2}$, the synthesis rates $s_x = s_y = 50$, the degradation rates $d_x = d_y = 1$, and unbinding rates $u_x = u_y = 0.1$. At the steady state, there are three probability peaks located at $(X, Y) = (0, 0), (50, 0), (0, 50)$, corresponding to the states of the genes G_x and G_y of "Off-Off" $(x = 0, y = 0)$, "On-Off" $(x = 1, y = 0)$, and "Off-On" $(x = 0, y = 1)$ (Figure 2A, 2D and 2G).

The steady state probability distribution of reactions R_1, R_3 given $x = 1$ (Eqn. (16)), which are birth-and-death processes, is the Poisson distribution with the maximum at its expected value of $X = s_X/d_X = 50$[73]. Similarly, the steady state probability distribution for the birth-and-death process of reactions (R_2, R_4) given $y = 1$, (Eqn. (16)), is the Poisson distribution with the maximum at its expected value of $Y = s_Y/d_Y = 50$. When the binding reaction has a higher propensity than unbinding, the genetic state "On-On" $(x = 1, y = 1)$ disappears. With the multiplication factor of the copy number of molecules, this occurs even when b_y is an order of magnitude smaller than u_y.

From computed $p(X, Y, x, y)$, we show its projection to the plane of (X, Y) in Figure 2, namely, we show $p(X, Y) = p(X, Y, 0, 0) + p(X, Y, 1, 0) + p(X, Y, 0, 1) + p(X, Y, 1, 1)$. Similarly, $\mathbf{J}_s(X, Y)$, $\mathbf{J}_L(X, Y)$, $\mathbf{J}_{FP}(X, Y)$, $\mathbf{v}_s(X, Y)$, $\mathbf{v}_L(X, Y)$, and $\mathbf{v}_{FP}(X, Y)$ are shown as projected in Figure 2.

The steady-state probability surfaces in $-\log p(\mathbf{x}, t)$ is shown in Figure 2A, 2D and 2G, with high probability regions in red, and regions where probability is close to zero in white. The trajectories of the flux field at the steady state are shown in blue for the universal discrete flux field $\mathbf{J}_s(\mathbf{x}, t)$ in Figure 2A– 2C, for the Liouville flux field $\mathbf{J}_L(\mathbf{x}, t)$ in Figure 2D– 2F, and for the Fokker-Planck flux field $\mathbf{J}_{FP}(\mathbf{x}, t)$ in Figure 2G– 2I. In Figures 2B, 2E and 2H, regions with large absolute values of flux are shown in purple, and regions with small absolute values of flux are shown in turquoise blue. In Figures 2C, 2F and 2I, regions with large absolute values of flux are shown in turquoise blue regions with small absolute values of velocity are shown in purple.

1. Universal Discrete Stochastic Flux and Velocity fields

The heatmaps of the universal discrete probability flux in $\log|\mathbf{J}_s(\mathbf{x}, t)|$ and velocity in $\log|\mathbf{v}_s(\mathbf{x}, t)|$ (Figure 2B and Figure 2C, respectively) show that locations with larger flux values also have higher probability. The states "Off-Off", "On-Off", and "Off-On" can be regarded as attractors of the probability flux. The flux lines converge to the regions of states near "On-Off" and "Off-On", after first reaching the state "Off-Off". Figure 2C of $\log|\mathbf{v}_s(X, Y)|$ shows that the velocity has larger values at locations where the flux trajectories are close to be straight lines (purple regions, Figure 2C), but drops significantly when the trajectories make turns (turquoise regions, Figure 2C).

2. Liouville Flux for the Toggle Switch Network

In Liouville flux, larger values are associated with higher probabilities (Figure 2D – 2E). The states "On-Off" and "Off-On" are the sinks. The flux and velocity lines converge to the states "On-Off" and "Off-On",

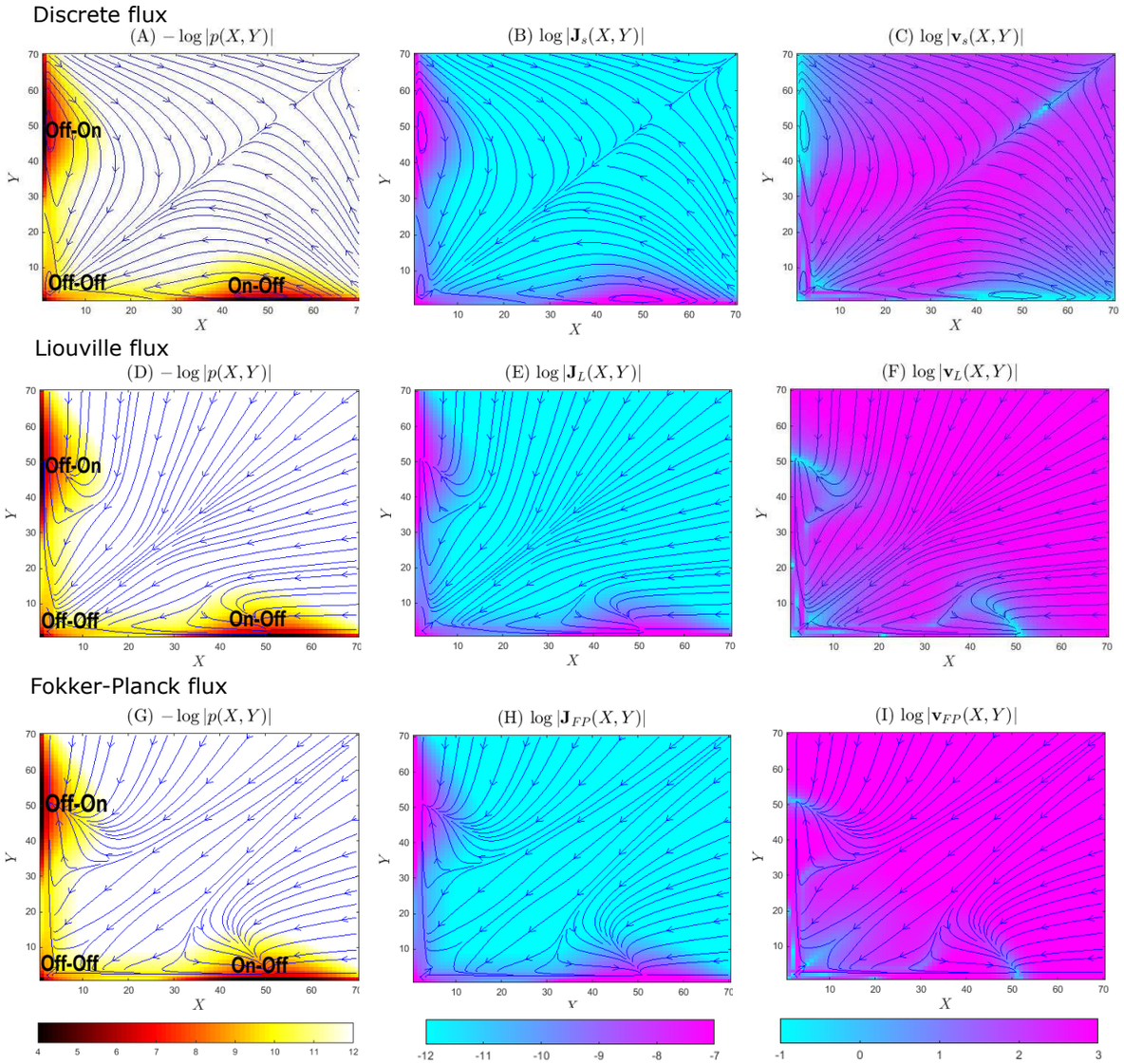

FIG. 2. The probability surfaces, fluxes, and velocities of the toggle switch system with strong promoter binding ($b = 1 \times 10^{-2}$) at the steady state. Probability value is given by the color scale, and the fluxes/velocities are shown in blue solid lines. The discrete stochastic flux model with probability surface in $-\log(p(x,y))$ (A), flux in $\log|\mathbf{J}_s(x,y)|$ (B), and velocity in $\log|\mathbf{v}_s(x,y)|$ (C); the Liouville flux model with probability surface in $-\log(p(x,y))$ (D), flux in $\log|\mathbf{J}_L(x,y)|$ (E), and velocity in $\log|\mathbf{v}_L(x,y)|$ (F); and the Fokker-Planck flux model with probability surface in $-\log(p(x,y))$ (G), flux in $\log|\mathbf{J}_{FP}(x,y)|$ (H), and velocity in $\log|\mathbf{v}_{FP}(x,y)|$ (I).

after first reaching towards the state "Off-Off". These patterns are the same as that of the universal discrete flux (Figure 2A). Detailed examination shows that the flux sinks are located at the states $(X = 50, Y = 0)$ and $(X = 0, Y = 50)$. These are local maxima of the probability surface. The absolute value of velocity function $\log|\mathbf{v}_L(X,Y)|$ shows that the probability velocity has larger values at locations where the flux trajectories are close to be straight lines (purple regions, Figure 2F), but drops significantly when the trajectories make turns (turquoise regions, Figure 2F).

While Liouville flux trajectories and the universal discrete flux trajectories depict overall similar behavior of the system. The flux lines converge to the states "Off-On" and "On-Off" after going through the state "Off-Off", an intermediate attractor of the flux, there are significant differences. The sinks at "Off-On" and "On-Off" are single states of $(X = 50, Y = 0)$ and $(X = 0, Y = 50)$ in Liouville flux (Figure 2F), but they are regions consisting of states in discrete flux close to $(X = 50, Y = 0)$ and $(X = 0, Y = 50)$, where the flux trajectories fluctuate (Figure 2C). The flux trajectories for the Liouville flux

start at the source located at $(+\infty, +\infty)$. This is different from the discrete flux, where the trajectories starting from the states with sufficiently large copy numbers converge to a sink at $(+\infty, +\infty)$, although these states have very small probability mass.

3. Fokker-Planck flux for the Toggle Switch Network

In the heat map of the Fokker-Planck probability flux, larger values are associated with higher probabilities (Figure 2G – 2I). The states "Off-Off", "On-Off", and "Off-On" are attractors of the flux. The velocity and flux lines converges to the states "On-Off" and "Off-On", after first reaching the state "Off-Off". These are the same as the Liouville flux and similar to the discrete flux (Figure 2A and 2D). Flux sinks are located at the states "On-Off" and "Off-On", represented by a single states $(X = 50, Y = 0)$ and $(X = 0, Y = 50)$ as in the case of Liouville flux. These two states correspond to the maxima of the Poisson distribution of the birth-and-death process (Eqn. (16)) of reactions (R_1, R_3) given $x = 1$, and (R_2, R_4) given $y = 1$, respectively. The absolute value of velocity function $\log|\mathbf{v}_L(X, Y)|$ shows that the velocity has larger values at locations where the flux trajectories are close to be straight lines (purple regions on Figure 2F), but drops significantly when the trajectories make turns (turquoise regions on Figure 2I).

There are significant differences between the Fokker-Planck flux and the discrete stochastic flux. The states "Off-On" and "On-Off" are single states with $(X = 50, Y = 0)$ and $(X = 0, Y = 50)$ in Fokker-Planck flux (Figure 2F)), but they involve sets of the states close to $(X = 50, Y = 0)$ and $(X = 0, Y = 50)$ in discrete flux (Figure 2C).The source of the flux for the Fokker-Planck flux is located at $(+\infty, +\infty)$ at the infinity. This is again different from the universal discrete stochastic flux, where a sink is at $(+\infty, +\infty)$.

The Liouville flux trajectories and the Fokker-Planck trajectories depict similar behavior, but with some differences. Starting from the same initial locations, for instance, $(X = 70, Y = 40)$ or $(X = 40, Y = 70)$, the Liouville trajectories first tend to reach the state "Off-Off" and then converge to the states "On-Off" or "Off-On". In contrast, the Fokker-Planck flux starting from the same states tends to converge to the "Off-On" or the "On-Off" directly.

4. Flux in Different Genetic States

While previous discussions are based on projections in the (X, Y) plane with different genetic states of (x, y) marginalized, we now examined fluxes in each of the specific genetic states of genes x and y, namely, the "Off-Off" state at the gene copy number of $(x = 0, y = 0)$ (Figure 3A, 3D, 3G), the "On-Off" state at $(x = 1, y = 0)$ (Figure 3B, 3E, 3H), and the "On-On" state at $(x = 1, y = 1)$ (Figure 3C, 3F, 3I). We neglect the case of $(x = 0, y = 1)$ as it is symmetric to that of $(x = 1, y = 0)$.

At the "Off-Off" state $(x = 0, y = 0)$, we observe the existence of a sink at $(X = 0, Y = 0)$ for all three models of fluxes (Figure 3A, 3D, and 3G). This is expected, as it is the state where both genes are bound, and the probability distribution has a peak. The Fokker-Planck and the Liouville flux trajectories converge to the state $(X = 0, Y = 0)$ (Figure 3D) following straight lines evenly spread out in the X–Y plane, whereas the discrete flux trajectories bend toward the axes of $X = 0$ and $Y = 0$.

At the "On-Off" state $(x = 1, y = 0)$, we observe the existence of the flux sink at $(X = 50, Y = 0)$ for the Liouville and Fokker-Planck models (Figure 3E and 3H). The discrete stochastic flux trajectories converge to an area consisting states near $(X = 50, Y = 0)$ (Figure 3B).

At the"On-On" state, where $X \in [40, 60]$ and $Y \in [40, 60]$, both genes are unbound and there is overall a small amount of probability mass associated with this genetic state. The three flux models give markedly different results, with sinks located at very different locations. The Liouville flux has the sink at $(X = 39, Y = 39)$ (Figure 3F). There are three sinks for the Fokker-Planck flux (Figure 3I). The discrete flux appears to have the sink at $(+\infty, +\infty)$ (Figure 3C).

It is informative to examine the behavior of the system with high copy number of P_X and P_Y in the regime where the law of mass action applies. We can obtain that critical points for each of the four genetic states. For the "On-On" state, we have $\langle X\rangle = (-d_X + \sqrt{d_X^2 + 4s_X b_y})/(2b_y) \approx 37$, $\langle Y\rangle = (-d_Y + \sqrt{d_Y^2 + 4s_Y b_x})/(2b_x) \approx 37$. For the "On-Off" state, we have $\langle X\rangle = (s_X + u_y)/d_X \approx 50$, $\langle Y\rangle = 0$. For the "Off-On" state, we have $\langle X\rangle = 0$, $\langle Y\rangle = (s_Y + u_x)/d_Y \approx 50$. For the "Off-Off" state, we have $\langle X\rangle = (u_x)/d_X \approx 0$, $\langle Y\rangle = u_y/d_Y \approx 0$. The eigenvalues for all four critical points are negative, indicating that all four are sinks. At the states "On-On" and "Off-Off", the eigenvalues are equal and matrices are multiples of the unit matrix, then flux lines form a star.[74]

These critical points are exactly where the sinks of Liouville flux located. The sink $(X = 0, Y = 0)$ at the state "Off-Off" exists for all flux models. The sink at $(X = 50, Y = 0)/(X = 0, Y = 50)$ for the "On-Off"/"Off-On" state exists for the Liouville and Fokker-Planck models. In contrast, the discrete flux lines converge to a broader set of states near the peak $(X = 50, Y = 0)$ $((X = 0, Y = 50))$. For the "On-On" state, the Liouville flux converges to the sink at $(X \approx 37, Y \approx 37)$, while there are multiple sinks for Fokker-Planck flux. The discrete flux does not converge to a single sink.

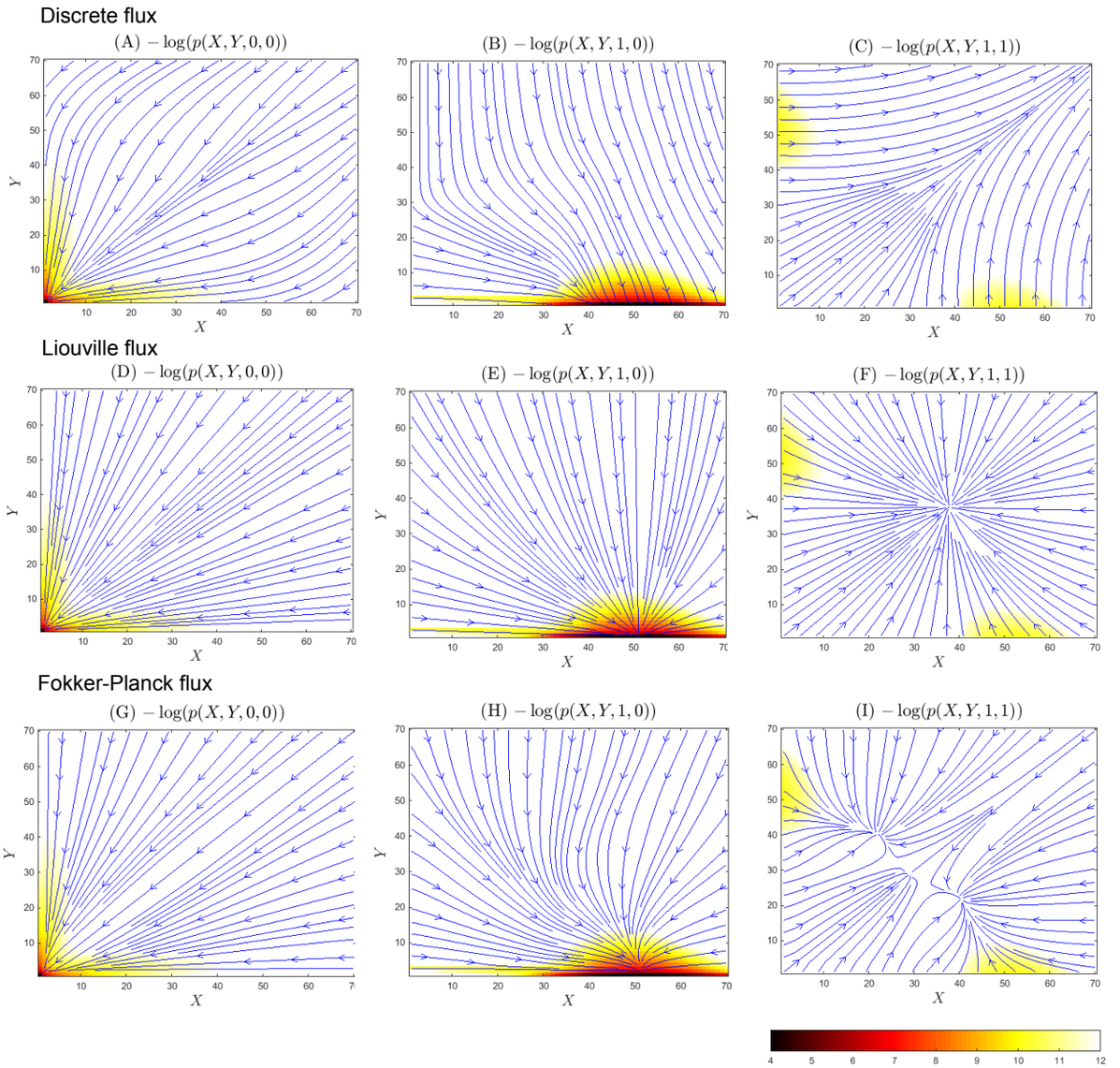

FIG. 3. Fluxes of the toggle switch system described at strong promoter binding of $b = 1 \times 10^{-2}$. The "Off-Off"gene state ($x = 0, y = 0$): (A) heat map of $-\log p(X,Y,0,0)$ and flux lines of $\mathbf{J}_s(X,Y,0,0)$, (D) heat map of $-\log p(X,Y,0,0)$ and flux lines of $\mathbf{J}_L(X,Y,0,0)$, and (G) heat map of $-\log p(X,Y,0,0)$ and flux lines of $\mathbf{J}_{FP}(X,Y,0,0)$; The "On-Off"gene state ($x = 1, y = 0$): (B) heat map of $-\log p(X,Y,1,0)$ and flux lines of $\mathbf{J}_s(X,Y,1,0)$, (E) heat map of $-\log p(X,Y,1,0)$ and flux lines of $\mathbf{J}_L(X,Y,1,0)$, and (H) heat map of $-\log p(X,Y,1,0)$ and flux lines of $\mathbf{J}_{FP}(X,Y,1,0)$; The "On-On"gene state ($x = 1, y = 1$): (C) heat map of $-\log p(X,Y,1,1)$ and flux lines for $\mathbf{J}_s(X,Y,1,1)$, (F) heat map of $-\log p(X,Y,1,1)$ and flux lines for $\mathbf{J}_L(X,Y,1,1)$, (I) heat map of $-\log p(X,Y,1,1)$ and flux lines for $\mathbf{J}_{FP}(X,Y,1,1)$.

C. Flux and velocity fields in the toggle switch with weak promoter binding from three methods

We now consider the system with weak promoter binding. The binding rates are $b_x = b_y = 1 \times 10^{-4}$, the synthesis rates $s_x = s_y = 50$, the degradation rates $d_x = d_y = 1$, and unbinding rates $u_x = u_y = 0.1$. At the steady state, there are four probability peaks located at $(X,Y) = (0,0)$, $(50,0)$, $(0,50)$,and $(50,50)$, corresponding to the states of genes G_x and G_y of "Off-Off" ($x = 0, y = 0$), "On-Off" ($x = 1, y = 0$), "Off-On" ($x = 0, y = 1$), and "On-On" ($x = 1, y = 1$) (Figure 4A, 4D and 4G). The steady state probability distribution for the birth-and-death process of reactions (R_1, R_3) of Eqn. (16), given $x = 1$, is the Poisson distribution with the maximum at its expected value of $X = s_X/d_X = 50$[73]. Similarly, the steady state probability distribution for the birth-and-death process of reactions (R_2, R_4) given $y = 1$, is the Poisson distribution

with the maximum at its expected value of $Y = s_Y/d_Y = 50$. From computed $p(X, Y, x, y)$, we show $p(X, Y)$, $\mathbf{J}_s(X, Y)$, $\mathbf{J}_L(X, Y)$, $\mathbf{J}_{FP}(X, Y)$, $\mathbf{v}_s(X, Y)$, $\mathbf{v}_L(X, Y)$, and $\mathbf{v}_{FP}(X, Y)$ projected on the plane of (X, Y) in Figure 4.

The steady-state probability surfacse in $-\log p(\mathbf{x}, t)$ is shown in Figure 4A, 4D and 4G, where high probability regions are in red, and regions where probability is close to zero in white. The trajectories of the flux field at the steady state are shown in blue for the universal discrete flux field $\mathbf{J}_s(\mathbf{x}, t)$ in Figure 4A– 4C, for the Liouville flux field $\mathbf{J}_L(\mathbf{x}, t)$ in Figure 4D– 4F, and for the Fokker-Planck flux field $\mathbf{J}_{FP}(\mathbf{x}, t)$ in Figure 4G– 4I. In Figure 4B, 4E and 4H, regions with large absolute values of flux are shown in purple, and regions with low absolute values of flux are shown in turquoise blue. In Figure 4C, 4F and 4I, regions with large absolute values of velocity are shown in turquoise blue. In Figure 4B, 4E and 4I, regions with small absolute values of velocity are shown in purple.

1. Universal Discrete Stochastic Flux and Velocity fields

The heatmaps of the universal discrete probability flux in $\log|J_s(\mathbf{x}, t)|$ and velocity in $\log|v_s(\mathbf{x}, t)|$ are shown in Figure 4B and Figure 4C, respectively. We note that locations with larger flux values also have higher probability. Unlike the previous case of strong promoter binding, we observe the presence of stochastic oscillations around both "On-Off" and "Off-On" states. In addition to the oscillations between the states "Off-On" ("On-Off") and "On-On", the system also fluctuates from the state "On-On" to "Off-Off", and then to "Off-On"/"On-Off". Figure 4C of $\log|\mathbf{v}_s(X, Y)|$ shows that the velocity drops significantly when the trajectories make turns (turquoise regions, Figure 4C).

There are more states with large flux values compared to the condition of strong promoter binding, *i.e.*, there are more purple regions of higher probability mass in Figure 4B than in Figure 2B. With more distributed probability mass and the observation of oscillations, the steady state of the toggle switch system with weak promoter binding is overall markedly less stable than that with strong promoter binding.

2. Liouville Flux

In the heat map of Liouville flux, larger values are associated with higher probabilities (Figure 4D – 4E). The states "Off-Off", "On-Off", "Off-On" and "On-On" are the attractors of the flux. While stochastic discrete flux exhibits strong oscillations, Liouville flux trajectories converge to the probability peak at the "On-On" state after travelling through peaks at "On-Off", "Off-On", and "Off-Off" states. The source of the flux is at both infinity and at the state $(X = 35, Y = 35)$. The sink is located at the states $(X = 49, Y = 49)$. The absolute values of velocity function $\log|\mathbf{v}_L(X, Y)|$ are larger at locations where the flux trajectories are close to straight lines (purple regions, Figure 4F), but drop significantly when the trajectories make turns (turquoise regions on Figure 4F).

The Liouville flux trajectories and the universal discrete flux trajectories exhibit significantly different behavior. Due to fast unbinding relative to binding at this condition of prominent stochasticity, the toggle switch system constantly alternate between the bounded and unbounded states for genes x and y. However, this phenomena is not captured by the Liouville flux.

3. Fokker-Planck Flux for the Toggle Switch Network

In the heat map of the Fokker-Planck probability flux, larger values are associated with higher probabilities (Figure 4G– 4I). The states "Off-Off", "On-Off", "Off-On" and "On-On" are the attractors of the flux. While stochastic discrete flux exhibits strong oscillations, Fokker-Planck flux trajectories, as Liouville flux, converge to the probability peak at the "On-On" state after travelling through peaks at "On-Off", "Off-On", and "Off-Off" states. The source of the flux is at both infinity and at the state $(X = 30, Y = 30)$. The sink is located at the states $(X = 50, Y = 50)$. The absolute value of velocity function $\log|\mathbf{v}_L(X, Y)|$ are larger at locations where the flux trajectories are close to straight lines (purple regions on Figure 4I), but drop significantly when the trajectories make turns (turquoise regions on Figure 4I).

The Liouville flux trajectories and the Fokker-Planck trajectories depict almost identical behavior of the system. There are some small differences. The sink for the gene state $(x = 1, y = 1)$ for the Liouville flux is at $(X = 49, Y = 49)$, which is different for the sink for the Fokker-Planck flux, which is at $(X = 50, Y = 50)$ (Figure 4G – 4I). There are significant differences between the Fokker-Planck flux and the discrete stochastic flux. Whereas stochastic discrete flux exhibits oscillations, Fokker-Planck flux trajectories converge to the system probability peak at the state "On-On" $(X = 50, Y = 50)$

4. Flux in Different Genetic States

We now examined the fluxes in each of the specific genetic states. At the "Off-Off" state $(x = 0, y = 0)$ (Figure 5A, 5D, 5G), we observe the existence of the sink at $(X = 0, Y = 0)$ for all three models of fluxes. This is expected, as it is the state where both genes are bound, and the probability peak is located at $(X = 0, Y = 0)$. The Fokker-Planck and the Liouville flux trajectories converge to this state $(X = 0, Y = 0)$ following straight lines, which are evenly spread off in the $X - Y$ plane,

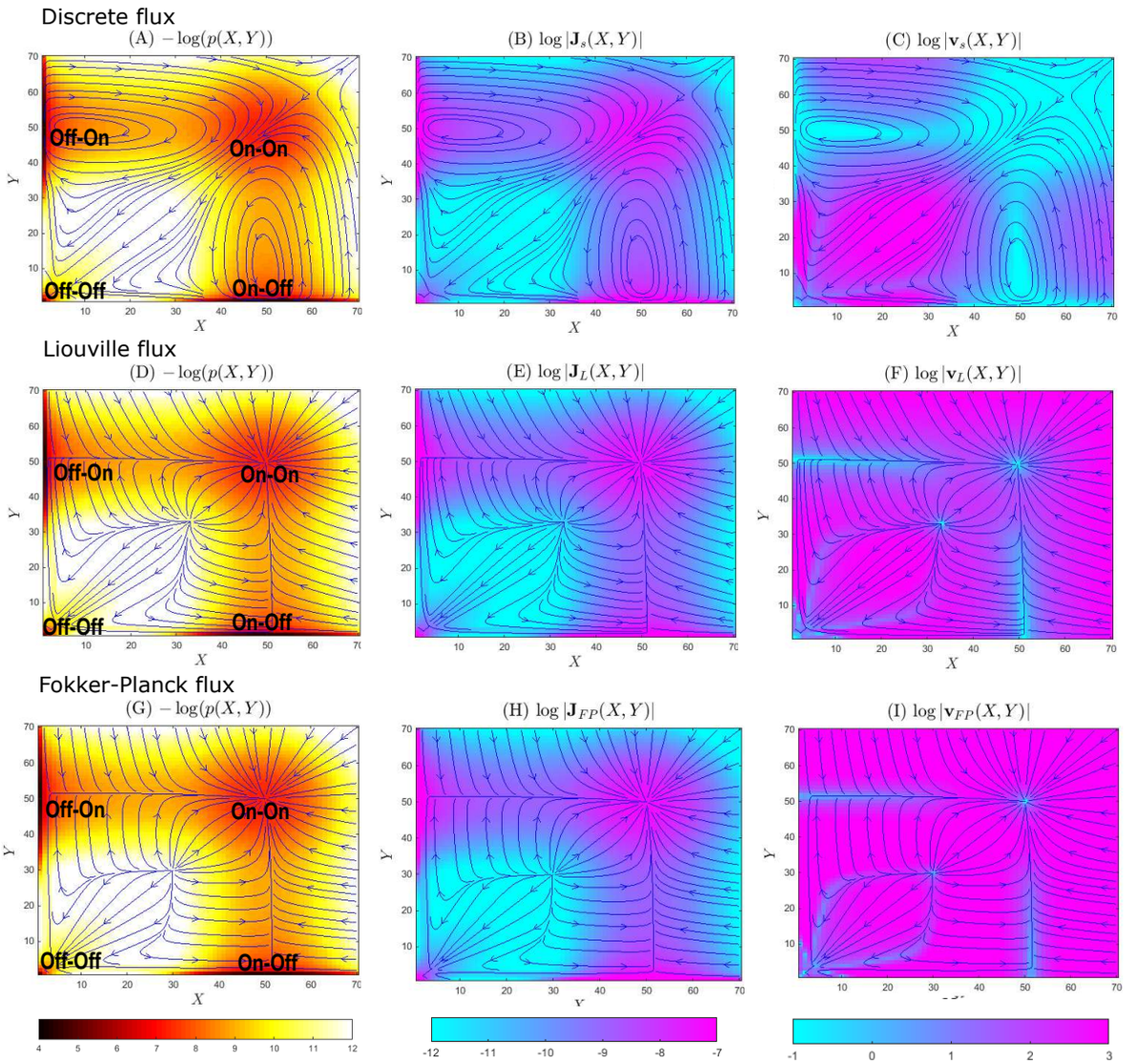

FIG. 4. The probability surfaces, fluxes, and velocities of the toggle switch system with weak promoter binding ($b = 1\times10^{-4}$) at the steady state. Probability value is given by the color scale, and the fluxes/velocities are shown in blue solid lines. The discrete stochastic flux model with probability surface in $-\log(p(x,y))$ (A), flux in $\log|\mathbf{J}_s(x,y)|$ (B), and velocity in $\log|\mathbf{v}_s(x,y)|$ (C); the Liouville flux model with probability surface in $-\log(p(x,y))$ (D), flux in $\log|\mathbf{J}_L(x,y)|$ (E), and velocity in $\log|\mathbf{v}_L(x,y)|$ (F); and the Fokker-Planck flux model with probability surface in $-\log(p(x,y))$ (G), flux in $\log|\mathbf{J}_{FP}(x,y)|$ (H), and velocity in $\log|\mathbf{v}_{FP}(x,y)|$ (I).

whereas the discrete flux trajectories bend toward the axes of $X = 0$ and $Y = 0$.

At the "On-Off" state ($x = 1, y = 0$) (Figure 5B, 5E, 5H), we observe the existence of a flux sink at ($X = 50, Y = 0$) for the Liouville and Fokker-Planck models (Figure 5D and 5E). The discrete stochastic flux trajectories converge to an area of states near ($X = 50$, $Y = 0$).

At the "On-On" state where both genes are unbound (Figure 5C, 5F, and 5I), the three flux models give markedly different results, with sinks at different locations. The Liouville flux has the sink at ($X = 50, Y = 50$) (Figure 5F), and the Fokker-Planck flux has the sink at ($X = 49, Y = 49$) (Figure 5I). The discrete flux appears to have a sink at $(+\infty, +\infty)$ (Figure 5C).

It is informative to examine the condition of high copy numbers of P_X and P_Y, where the law of mass action applies. We can obtain the critical points for each of the four genetic states. For the state "Off-Off", we have $\langle X\rangle = u_x/d_X \approx 0$, $\langle Y\rangle = u_y/d_Y \approx 0$. For the state "On-Off", we have $\langle X\rangle = (s_X + u_y)/d_X \approx 50$, $\langle Y\rangle = 0$. For the state "Off-On", we have $\langle X\rangle = 0$, $\langle Y\rangle = (s_Y + u_x)/d_Y \approx 50$. For the state "On-On", we have

$\langle X\rangle = (-d_X + \sqrt{d_X^2 + 4s_X b_y})/(2b_y) \approx 50$, $\langle Y\rangle = (-d_Y + \sqrt{d_Y^2 + 4s_Y b_x})/(2b_x) \approx 50$. The eigenvalues at all four critical points are negative, indicating that they are sinks. At the states "On-On" and "Off-Off", the eigenvalues are equal and matrices are multiples of the unit matrix, then flux lines form a star.[74]

These critical points are where the sinks of Liouville and Fokker-Planck fluxes located. The sink $(X = 0, Y = 0)$ at the state "Off-Off" exists for all flux models. For the "On-Off"/"Off-On" state, the sink at $(X = 50, Y = 0)/(X = 0, Y = 50)$ exists for the Liouville and Fokker-Planck fluxes, while the discrete flux lines converge to a set of the states near $(X = 50, Y = 0)$ $((X = 0, Y = 50))$. For the "On-On" state, the Liouville and Fokker-Planck fluxes converge to $(X = 50, Y = 50)$ and $(X = 49, Y = 49)$, respectively. The discrete stochastic flux does not converge to any sink.

III. STOCHASTIC FLUCTUATION AND OSCILLATIONS IN TOGGLE SWITCH

A. Strong promoter binding

With strong promoter binding ($b = 1\times10^{-2}$), the three flux models are overall similar, but with important differences in details. Discrete flux trajectories exhibit small fluctuations around the "On-Off"peak at $(X = 50, Y = 0)$ (and symmetrically at $(X = 0, Y = 50)$, Figure 6A). While changes in Y are just a handful copies of molecule, the amount of molecules of X fluctuates more significantly (Figure 6A).

To gain better understanding of the observed fluctuations, we examine reaction trajectories sampled using the SSA algorithm from the initial state of $(X = 50, Y = 0, x = 1, y = 0)$, where the "On-Off" peak is located. Figure 6B shows how trajectories of copy numbers of protein P_X (red lines) and protein P_Y (black lines) fluctuate. P_X fluctuates around $X = 50$. This is due to stochasticity in the synthesis and the degradation of P_X at the genetic state of $x = 1$. The trajectories of copy number of protein P_Y (black lines) also fluctuate around $Y = 0$, but with overall much smaller magnitude. This is because gene G_y occasionally becomes unbound $(X > 0)$, upon which P_Y is synthesized. However, since promoter binding is strong and at this condition P_X is in much larger amount then P_Y, gene G_y rapidly becomes inhibited by P_X again.

The fluctuations observed in reaction trajectories are well explained by the flux lines shown in Figure 6A, which form closed, x-axis-oriented horizontal ellipses around the state $(X = 50, Y = 0)$ (Figure 6A). The major axis of the ellipse corresponds to the stochastic fluctuations with larger magnitude in copies of P_X, and the minor axis to fluctuation with smaller magnitude in copies of P_Y.

While the behavior of stochastic fluctuation observed in reaction trajectories are well captured in the flowmap computed discrete stochastic flux, these fluctuations, however, are not captured by either the Liouville flux (Figure 6C) or the Fokker-Planck flux (Figure 6D), where both converge to a single state $(X = 50, Y = 0)$ (and symmetrically to $(X = 0, Y = 50)$).

B. Weak promoter binding

With weak promoter binding ($b = 1 \times 10^{-4}$), there are significant differences between the discrete flux and fluxes based on continuum approximations. The discrete flux lines (Figure 4A) exhibit strong oscillations between $(X = 50, Y = 50)$ and $(X = 50, Y = 0)$, and symmetrically between $(X = 50, Y = 50)$ and $(X = 0, Y = 50)$. Furthermore, probability flux also flows from $(X = 50, Y = 50)$ to $(X = 0, Y = 0)$, then to $(X = 50, Y = 0)$, and back to $(X = 50, Y = 50)$. Symmetric oscillatory pattern is also seen, where flux lines flow back to $(X = 50, Y = 50)$ via $(X = 0, Y = 0)$ and $(X = 0, Y = 50)$. In addition, occasionally oscillation can be seen between $(X = 50, Y = 0)$ and $(X = 0, Y = 50)$ via the state of $(X = 50, Y = 50)$.

To gain better understanding of the stochastic oscillations uncovered from the discrete flux model, we examine reaction trajectories sampled from the initial state of $(X = 50, Y = 0, x = 1, y = 0)$, where the "On-Off" peak is located. Figure 6F shows trajectories of copy number of protein P_X (red lines) and protein P_Y (black line). P_X fluctuates with small magnitude around $X = 50$. This is due to stochasticity in P_X synthesis and degradation at $x = 1$. This is similar to the fluctuation in P_X shown in Figure 6B where promoter binding is fast. P_Y exhibit similar fluctuation around $Y = 50$.

However, there is significant oscillation in P_Y (black line) of larger magnitude between $Y = 50$ and $Y = 0$. This is due to stochastic switching between the gene state of $y = 1$ and $y = 0$. Similarly, P_X (red) also oscillates between $X = 50$ and $X = 0$ due to switching between $x = 1$ and $x = 0$. Unlike that of strong promoter binding (Figure 6B), trajectory of P_Y (blackline) exhibit no fluctuations around $Y = 0$ (Figure 6F). This is because when gene G_y becomes unbound $(y = 1)$, the system has sufficient time to transit from $(Y = 0)$ to $(Y = 50)$ before gene G_y becomes bound again $(y = 0)$, as promoter binding of P_X to G_y is slow. Furthermore, the durations of simultaneous high copies of P_X and P_Y $(X = 50, Y = 50)$ are relatively short.

The oscillations observed in reaction trajectories are well-explained by the flowmap of the discrete flux (Figure 6E and Figure 4A). The closed vertical ellipses with foci at states $(X = 50, Y = 0)$ and $(X = 50, Y = 50)$ correspond to the larger stochastic fluctuations in Y (blackline) and smaller magnitute fluctuations in X (redline) (Figure 6F). Shown in Figure 4A but not in Figure 6E for clarity, the closed horizontal ellipses with foci at states $(X = 0, Y = 50)$ and $(X = 50, Y = 50)$ correspond to the larger stochastic fluctuations in X (redline) and

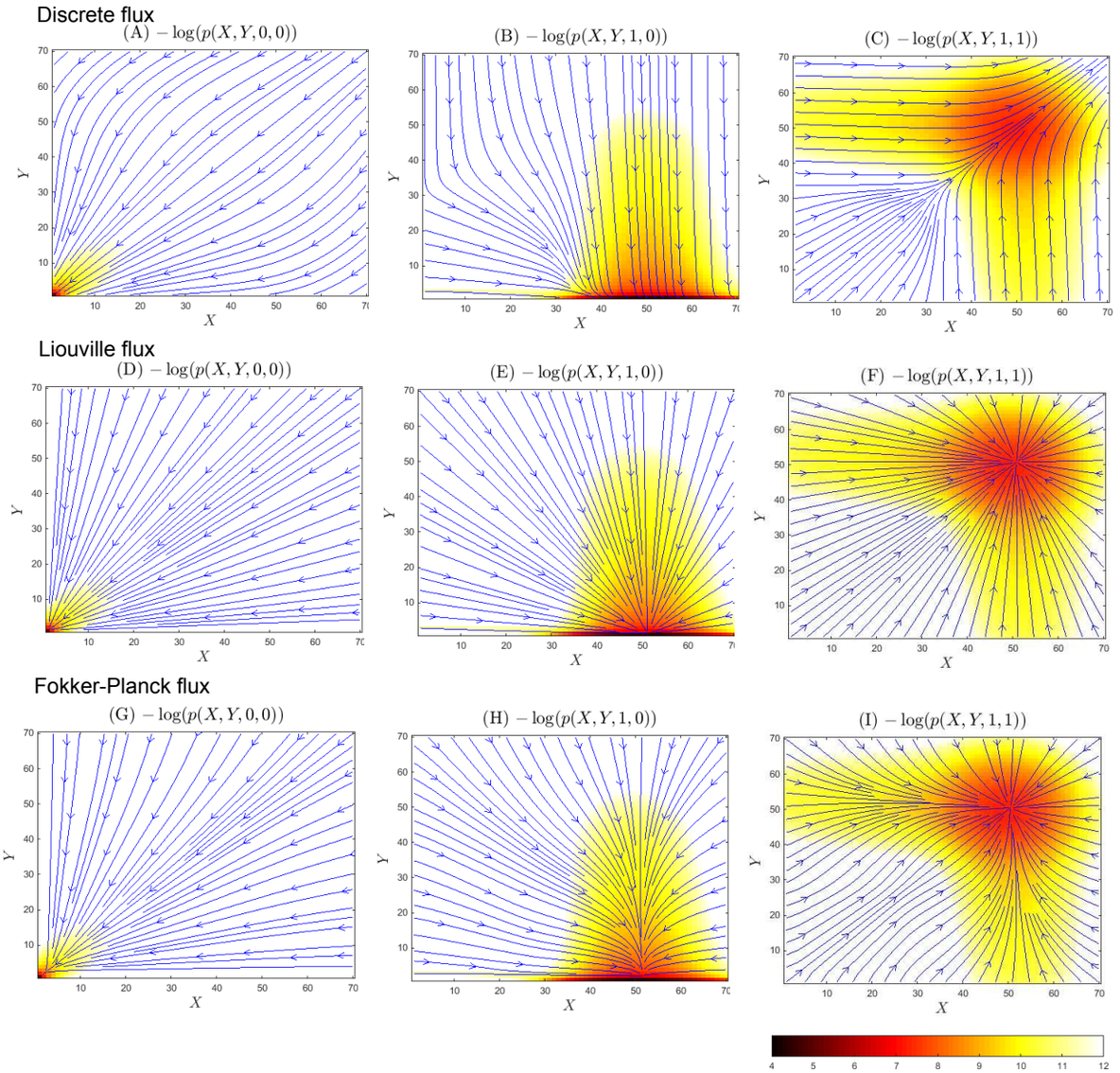

FIG. 5. Fluxes of the toggle switch system described at weak promoter binding of $b = 1 \times 10^{-4}$. The "Off-Off"gene state ($x = 0$, $y = 0$): (A) heat map of $-\log p(X,Y,0,0)$ and flux lines of $\mathbf{J}_s(X,Y,0,0)$, (D) heat map of $-\log p(X,Y,0,0)$ and flux lines of $\mathbf{J}_L(X,Y,0,0)$, and (G) heat map of $-\log p(X,Y,0,0)$ and flux lines of $\mathbf{J}_{FP}(X,Y,0,0)$; The "On-Off"gene state ($x = 1$, $y = 0$): (B) heat map of $-\log p(X,Y,1,0)$ and flux lines of $\mathbf{J}_s(X,Y,1,0)$, (E) heat map of $-\log p(X,Y,1,0)$ and flux lines of $\mathbf{J}_L(X,Y,1,0)$, and (H) heat map of $-\log p(X,Y,1,0)$ and flux lines of $\mathbf{J}_{FP}(X,Y,1,0)$; The "On-On"gene state ($x = 1$, $y = 1$): (C) heat map of $-\log p(X,Y,1,1)$ and flux lines for $\mathbf{J}_s(X,Y,1,1)$, (F) heat map of $-\log p(X,Y,1,1)$ and flux lines for $\mathbf{J}_L(X,Y,1,1)$, (I) heat map of $-\log p(X,Y,1,1)$ and flux lines for $\mathbf{J}_{FP}(X,Y,1,1)$.

smaller magnitute fluctuations in Y (blackline). Furthermore, corresponding to the shorter durations in trajectories when both P_X and P_Y are high at 50 (Figure 6F), the state ($X = 50$, $Y = 50$) indeed is a transient state in the flow maps of the discrete flux (Figure 4A– 4C).

Overall, the behavior of stochastic oscillations and fluctuations observed in reaction trajectories are well captured in the computed discrete stochastic flux. These oscillating behaviors, however, are not captured by either the Liouville flux (Figure 6C) or the Fokker-Planck flux (Figure 6D), where in either case the system converges to a single state of ($X = 50$, $Y = 50$).

IV. CONCLUSION

In this work, we studied three different models of probability flux, one directly based on the discrete chemical master equation (dCME), and two based on continuum approximation of the dCME. While continuum probabil-

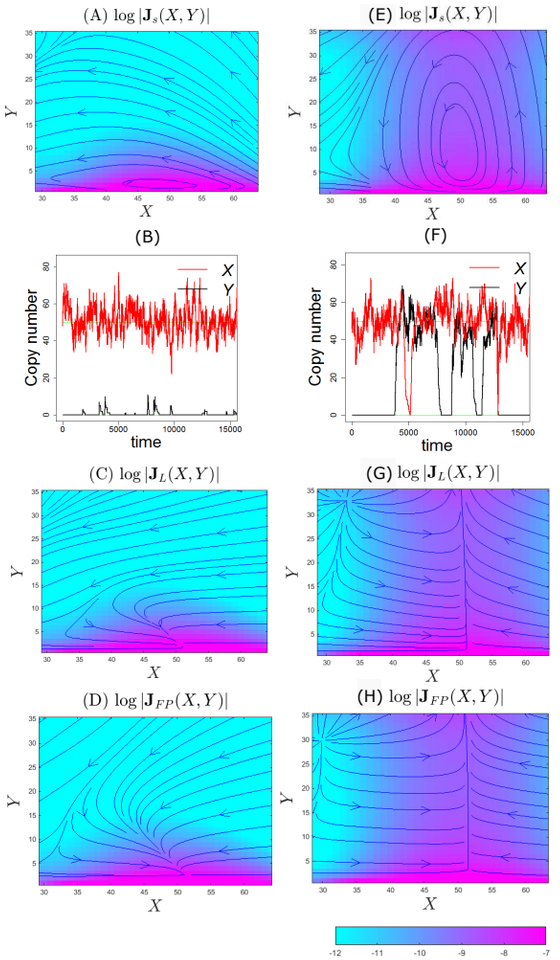

FIG. 6. The flow maps and trajectories of the probability fluxes of the toggle switch system near the state "On-Off", with strong promoter binding ($b = 1 \times 10^{-2}$) shown in $\log|\mathbf{J}_s(x,y)|$ (A), $\log|\mathbf{J}_L(x,y)|$ (C), $\log|\mathbf{J}_{FP}(x,y)|$ (D); and with weak promoter binding ($b = 1 \times 10^{-4}$) shown in $\log|\mathbf{J}_s(x,y)|$ (E), $\log|\mathbf{J}_L(x,y)|$ (G), $\log|\mathbf{J}_{FP}(x,y)|$ (H). Sampled Gillespie trajectories starting from the state ($X = 50$, $Y = 0$, $x = 1$, $y = 0$) are shown for strong binding (B) and for weak binding (F).

ity flux in stochastic models has been mostly based on Fokker-Planck formulations, we introduce here the Liouville flux based on mass-action kinetics. Using the toggle-switch system, we constructed global flow maps of probability flux at the non-equlibrium steady state for all three models.

Under the conditions when the rates of transcription factor to promoter binding are much faster than the unbinding rates, all three flux models show overall similar patterns, but with some important differences: the flux lines of the continuum models flow to single-states for both the "On-Off" and "Off-On" states (Figure 6C and 6D), while the flux lines of the discrete model form ellipses (Figure 6A), with better correspondence to the exhibited fluctuations of uneven magnitude in the two proteins as seen in SSA-generated reaction trajectories (Figure 6B). In region of large copy numbers of proteins, flux lines of the discrete model converge to infinity (Figure 2, 4), whereas the flux lines of continuum models converge to the sinks at "Off-Off", "On-Off" or "Off-On" states. States with large copy numbers have very low probability for the toggle switch system, and the behavior of the system in these states is not representative to the overall system behavior. Furthermore, examination of details of the flow maps at different genetic states reveal significant differences among these three models for the (1, 1) genetic state: the discrete flux flows to infinite, the Liouville flux flows to one sink, and the Fokker-Planck flux flows to three sinks.

Under the highly stochastic condition of slow promoter binding, the differences between the discrete and the continuum flux models are more prominent. The discrete flux model reveals the existence of stochastic oscillations, where flux lines form ellipses, with the "On-On" and "On-Off" states as foci, which are consistent with SSA-generated reaction trajectories. In contrast, both Fokker-Planck and Liouville fluxes converge to the "On-On" state and do not exhibit oscillatory behavior.

Over all, our results show that fluxes computed with these three differenting models can exhibit significantly different results. Although the Fokker-Planck flux model and the discrete flux model have been shown to have similar behavior in several well-studied networks, including the Schnakenberg system[23,36], this work reveals that there can be significant differences between them. Using the universal discrete stochastic flux model, we uncovered strong oscillating behavior of the toggle switch at the non-equilibrium steady state, which is due to strong fluctuations between binding and unbinding events. In contrast, Fokker-Planck and Liouville models fail to capture this phenomenon. Simulated stochastic trajectories fully confirmed findings obtained using the universal discrete models.

V. ACKNOWLEDGMENTS

Support from NIH R35 GM127084, NIH R01 CA204962 and NSF-DMS 1759536 is gratefully acknowledged. We thank an anonymous referee for helpful suggestions.

[1] H. Maamar, A. Raj, and D. Dubnau, Science **317**, 526 (2007).
[2] Y. Cao, H.-M. Lu, and J. Liang, Proceedings of the National Academy of Sciences (2010).
[3] M. Inui, G. Martello, and S. Piccolo, Nature Reviews. Molecular Cell Biology **11**, 252 (2010).
[4] J. E. Ferrell Jr, Current opinion in cell biology **14**, 140 (2002).
[5] K. Düvel, J. L. Yecies, S. Menon, P. Raman, A. I. Lipovsky, A. L. Souza, E. Triantafellow, Q. Ma, R. Gorski, S. Cleaver, and et al, Molecular cell **39**, 171 (2010).
[6] P. Érdi and J. Tóth, *Mathematical models of chemical reactions: theory and applications of deterministic and stochastic models* (Manchester University Press, 1989).

[7]M. B. Elowitz, A. J. Levine, E. D. Siggia, and P. S. Swain, Science **297**, 1183 (2002).
[8]P. S. Swain, M. B. Elowitz, and E. D. Siggia, Proceedings of the National Academy of Sciences **99**, 12795 (2002).
[9]T. G. Kurtz, Stochastic Processes and their Applications **6**, 233 (1978).
[10]D. T. Gillespie, The journal of physical chemistry **81**, 2340 (1977).
[11]J. Schnakenberg, Reviews of Modern physics **48**, 571 (1976).
[12]D. T. Gillespie, Physica A: Statistical Mechanics and its Applications **188**, 404 (1992).
[13]N. G. Van Kampen, *Stochastic processes in physics and chemistry*, Vol. 1 (Elsevier, 1992).
[14]D. T. Gillespie, Journal of computational physics **22**, 403 (1976).
[15]D. T. Gillespie, The Journal of Chemical Physics **113**, 297 (2000).
[16]B. J. Daigle Jr, M. K. Roh, D. T. Gillespie, and L. R. Petzold, The Journal of chemical Physics **134**, 01B628 (2011).
[17]Y. Cao and J. Liang, The Journal of Chemical Physics **139**, 07B605_1 (2013).
[18]B. Munsky and M. Khammash, J Chem Phys **124**, 044104 (2006).
[19]Y. Cao and J. Liang, BMC Systems Biology **2**, 30 (2008).
[20]R. Sidje and H. Vo, Mathematical Biosciences **269**, 10 (2015).
[21]Y. Cao, A. Terebus, and J. Liang, Bulletin of Mathematical Biology **78**, 617 (2016).
[22]Y. Cao, A. Terebus, and J. Liang, SIAM: Multiscale Modeling and Simulation (2016).
[23]L. Xu, H. Shi, H. Feng, and J. Wang, The Journal of Chemical Physics **136**, 165102 (2012).
[24]J. Wang, L. Xu, and E. Wang, Proceedings of the National Academy of Sciences **105**, 12271 (2008).
[25]R. Yuan, X. Wang, Y. Ma, B. Yuan, and P. Ao, Physical Review E **87**, 062109 (2013).
[26]Y. Tang, R. Yuan, and P. Ao, Physical Review E **89**, 062112 (2014).
[27]C. Li and J. Wang, Proceedings of the National Academy of Sciences **111**, 14130 (2014).
[28]C. Bianca and A. Lemarchand, Physica A: Statistical Mechanics and its Applications **438**, 1 (2015).
[29]B. C. Goodwin *et al.*, Temporal organization in cells. A dynamic theory of cellular control processes. (1963).
[30]H. H. McAdams and A. Arkin, Trends in Genetics **15**, 65 (1999).
[31]M. Strasser, F. J. Theis, and C. Marr, Biophysical Journal **102**, 19 (2012).
[32]J. T. Margaret, B. K. Chu, M. Roy, and E. L. Read, Biophysical Journal **109**, 1746 (2015).
[33]R. Zia and B. Schmittmann, Journal of Statistical Mechanics: Theory and Experiment **2007**, P07012 (2007).
[34]C. Li, E. Wang, and J. Wang, Biophysical Journal **101**, 1335 (2011).
[35]X.-J. Zhang, H. Qian, and M. Qian, Physics Reports **510**, 1 (2012).
[36]A. Terebus, C. Liu, and J. Liang, The Journal of Chemical Physics **149**, 185101 (2018).
[37]L. R. de Oliveira, A. Bazzani, E. Giampieri, and G. C. Castellani, The Journal of chemical Physics **141**, 08B608_1 (2014).
[38]J. Wang, L. Xu, E. Wang, and S. Huang, Biophysical Journal **99**, 29 (2010).
[39]C. Li and J. Wang, Journal of The Royal Society Interface **11**, 20140774 (2014).
[40]Y. Tang, R. Yuan, G. Wang, X. Zhu, and P. Ao, Scientific Reports **7**, 15762 (2017).
[41]T. L. Hill, *Free energy transduction and biochemical cycle kinetics* (Dover, Mineola, New York, 2005).
[42]T. Kurtz, J Appl Probab **8**, 344 (1971).
[43]D. J. Wilkinson, Nature Reviews Genetics **10**, 122 (2009).
[44]T. Szekely and K. Burrage, Computational and Structural Biotechnology Journal **12**, 14 (2014).
[45]A. Duncan, S. Liao, T. Vejchodskỳ, R. Erban, and R. Grima, Physical Review E **91**, 042111 (2015).
[46]R. Grima, P. Thomas, and A. V. Straube, The Journal of Chemical Physics **135**, 084103 (2011).
[47]P. Hanggi, H. Grabert, P. Talkner, and H. Thomas, Physical Review A **29**, 371 (1984).
[48]A. Ceccato and D. Frezzato, The Journal of chemical physics **148**, 064114 (2018).
[49]G. Karlebach and R. Shamir, Nature Reviews Molecular Cell Biology **9**, 770 (2008).
[50]C. Y. Mou, J.-l. Luo, and G. Nicolis, The Journal of Chemical Physics **84**, 7011 (1986).
[51]T. Schmiedl and U. Seifert, The Journal of Chemical Physics **126**, 044101 (2007).
[52]D. Schultz, A. M. Walczak, J. N. Onuchic, and P. G. Wolynes, Proceedings of the National Academy of Sciences **105**, 19165 (2008).
[53]A. Bazzani, G. C. Castellani, E. Giampieri, D. Remondini, and L. N. Cooper, The Journal of Chemical Physics **136**, 06B611 (2012).
[54]D. A. McQuarrie, Journal of applied probability **4**, 413 (1967).
[55]H. Kuwahara and I. Mura, The Journal of Chemical Physics **129**, 10B619 (2008).
[56]J. Keener and J. Sneyd, *Biochemical Reactions* (Springer, 1998).
[57]T. G. Kurtz, The Journal of Chemical Physics **57**, 2976 (1972).
[58]C. S. Gillespie, IET systems biology **3**, 52 (2009).
[59]P. Smadbeck and Y. N. Kaznessis, Proceedings of the National Academy of Sciences **110**, 14261 (2013).
[60]R. Shankar, *Principles of quantum mechanics* (Springer Science & Business Media, 2012).
[61]S. Xu, P. Sheng, and C. Liu, arXiv preprint arXiv:1408.4114 (2014).
[62]T. S. Gardner, C. R. Cantor, and J. J. Collins, Nature **403**, 339 (2000).
[63]R. Sekine, M. Yamamura, S. Ayukawa, K. Ishimatsu, S. Akama, M. Takinoue, M. Hagiya, and D. Kiga, Proceedings of the National Academy of Sciences **108**, 17969 (2011).
[64]M. Wu, R.-Q. Su, X. Li, T. Ellis, Y.-C. Lai, and X. Wang, Proceedings of the National Academy of Sciences **110**, 10610 (2013).
[65]G. Balázsi, A. van Oudenaarden, and J. J. Collins, Cell **144**, 910 (2011).
[66]J.-B. Lugagne, S. S. Carrillo, M. Kirch, A. Köhler, G. Batt, and P. Hersen, Nature Communications **8**, 1671 (2017).
[67]K.-Y. Kim and J. Wang, PLoS Computational Biology **3**, e60 (2007).
[68]D. Schultz, J. N. Onuchic, and P. G. Wolynes, The Journal of Chemical physics **126**, 06B613 (2007).
[69]J. Wang, J. Zhang, Z. Yuan, and T. Zhou, BMC Systems Biology **1**, 50 (2007).
[70]B. Verd, A. Crombach, and J. Jaeger, BMC Systems Biology **8**, 43 (2014).
[71]X. Fang, Q. Liu, C. Bohrer, Z. Hensel, W. Han, J. Wang, and J. Xiao, Nature communications **9**, 2787 (2018).
[72]P. B. Warren and P. R. ten Wolde, The Journal of Physical Chemistry B **109**, 6812 (2005).
[73]C. W. Gardiner *et al.*, *Handbook of stochastic methods*, Vol. 3 (springer Berlin, 1985).
[74]D. W. Jordan and P. Smith, *Nonlinear ordinary differential equations: an introduction to dynamical systems*, Vol. 2 (Oxford University Press, USA, 1999).
[75]T. B. Kepler and T. C. Elston, Biophysical journal **81**, 3116 (2001).
[76]D. T. Gillespie, The Journal of Physical Chemistry A **106**, 5063 (2002).

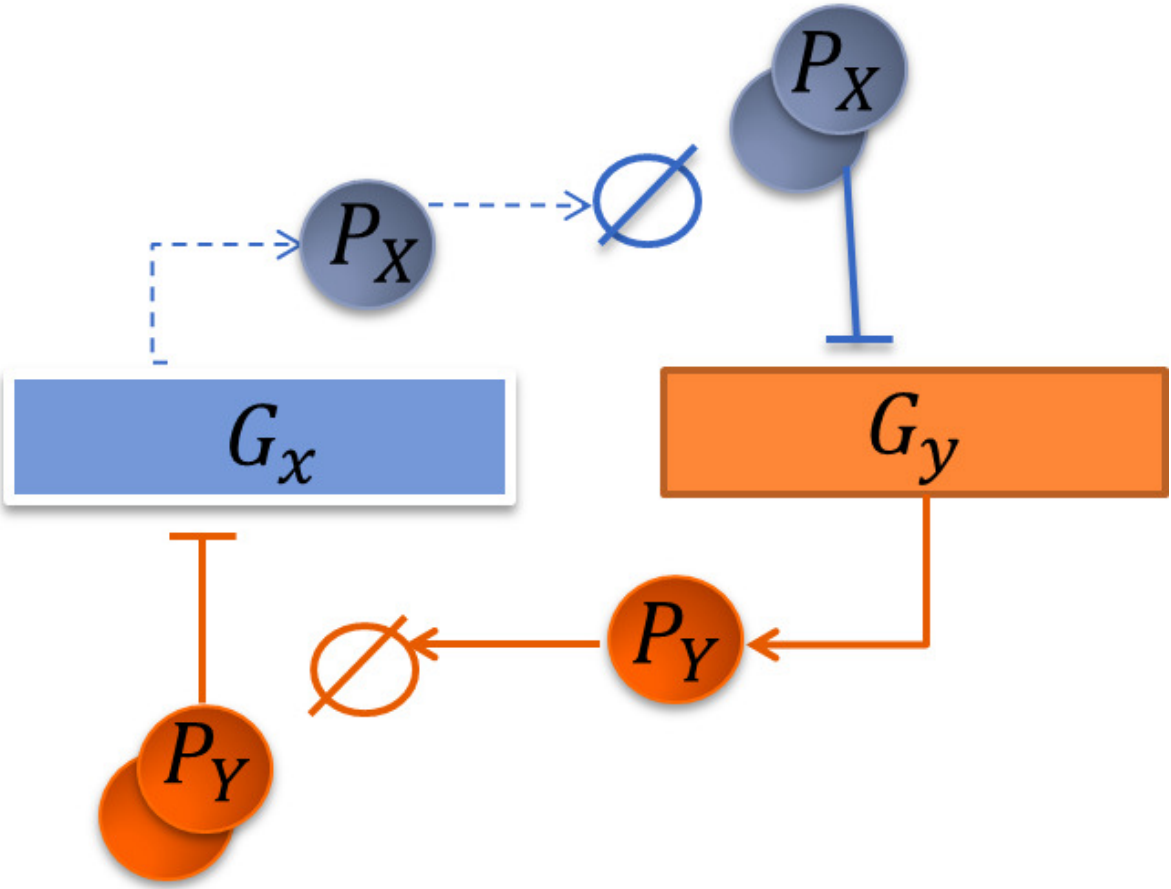
P_X
P_X
G_x
G_y
P_Y
P_Y

Discrete flux

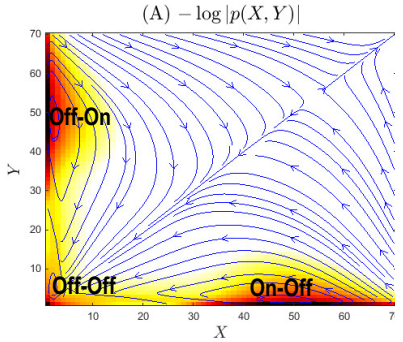

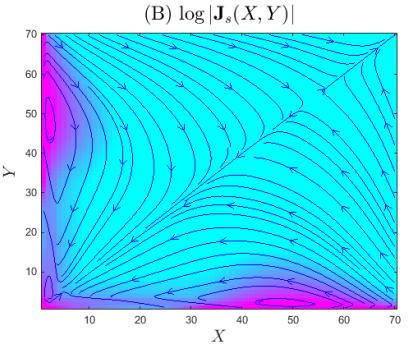

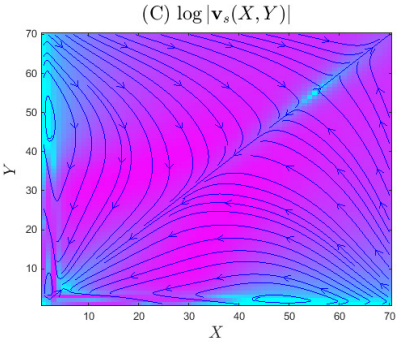

Liouville flux

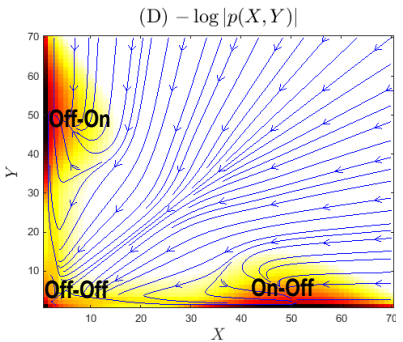

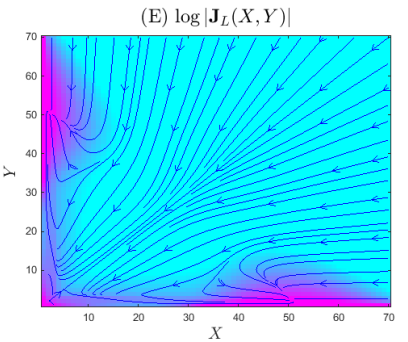

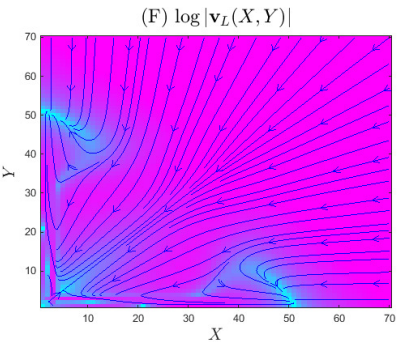

Fokker-Planck flux

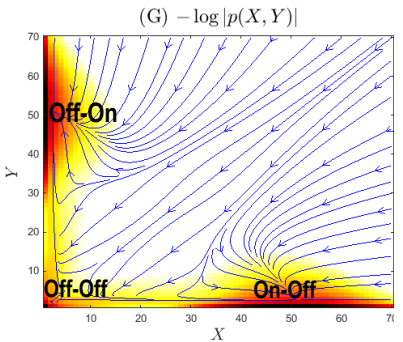

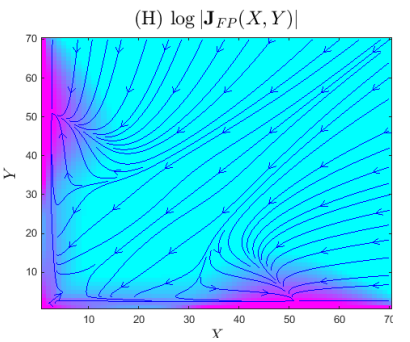

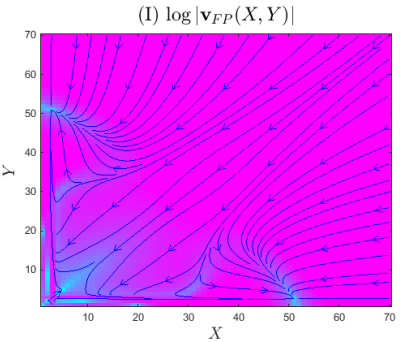

Discrete flux

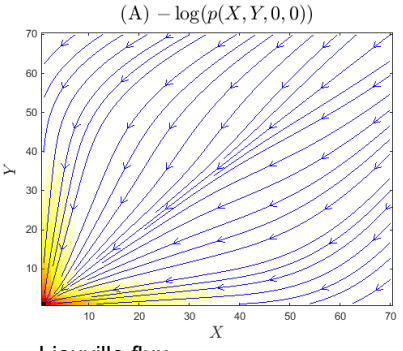

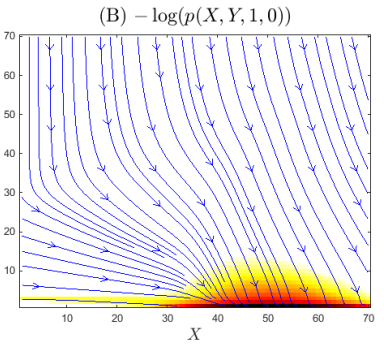

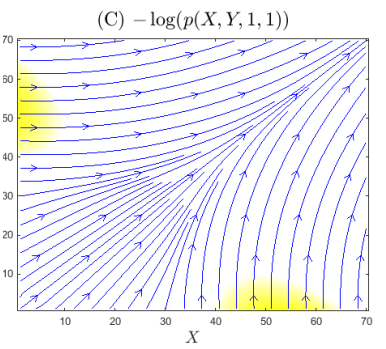

Liouville flux

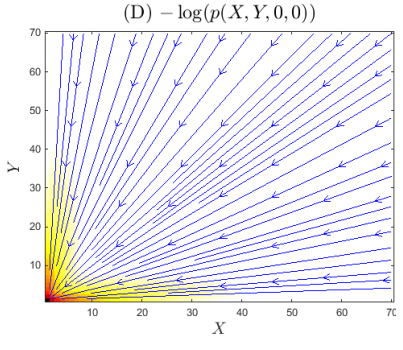

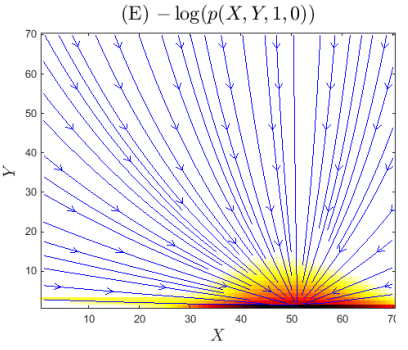

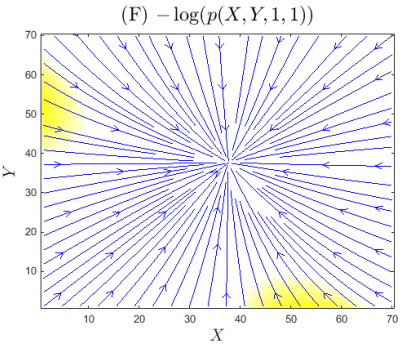

Fokker-Planck flux

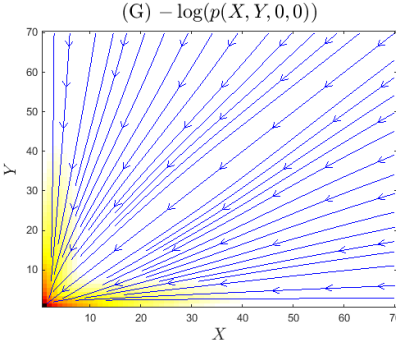

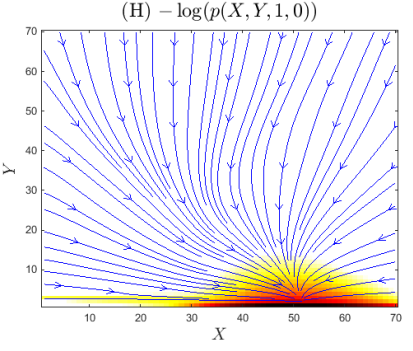

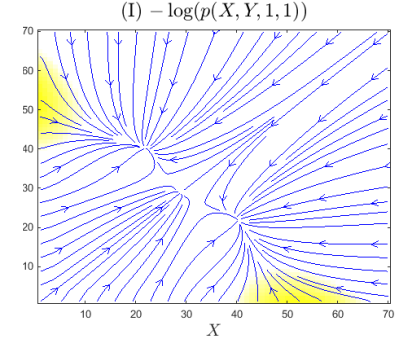

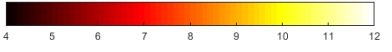

Discrete flux

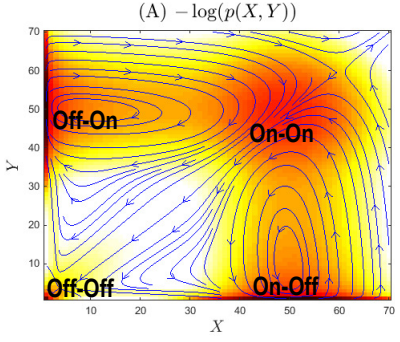

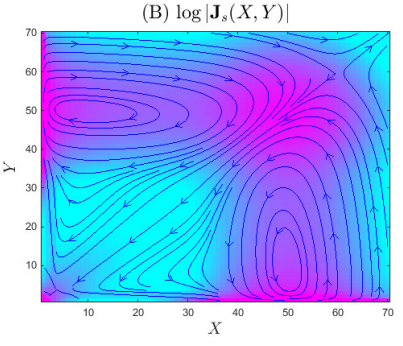

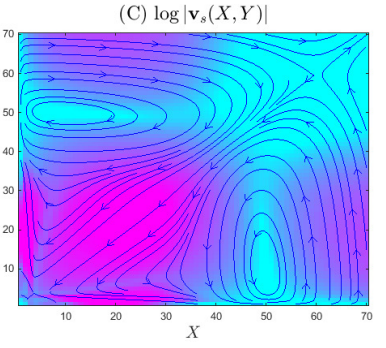

Liouville flux

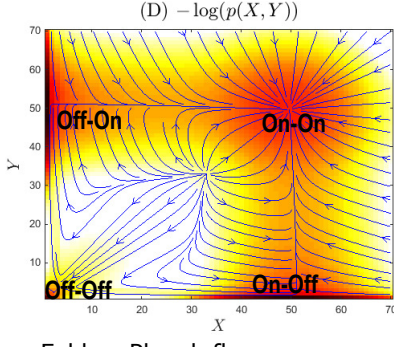

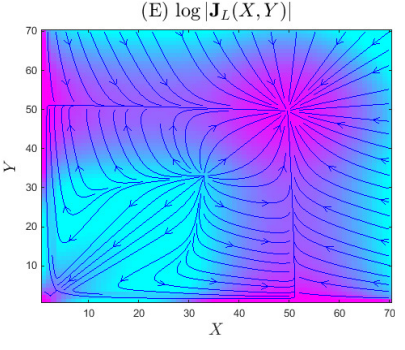

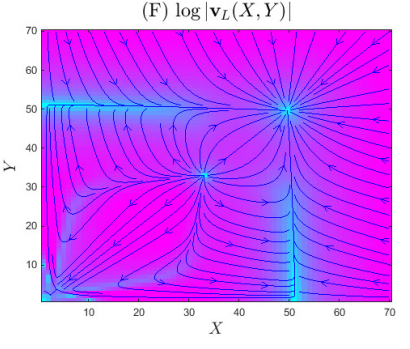

Fokker-Planck flux

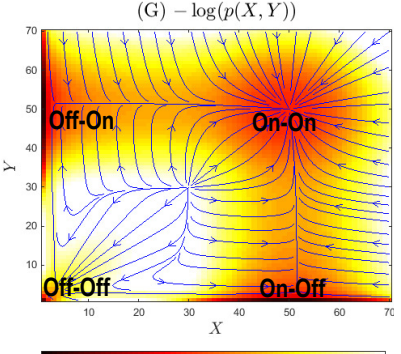

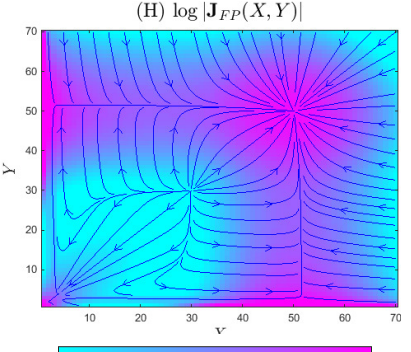

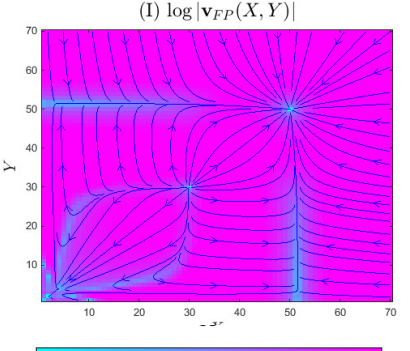

Discrete flux

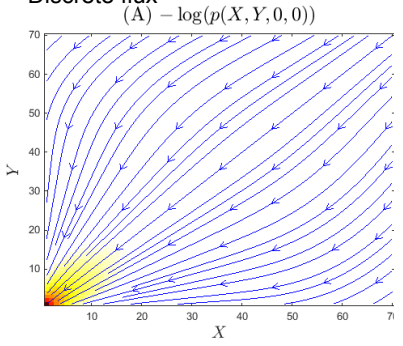

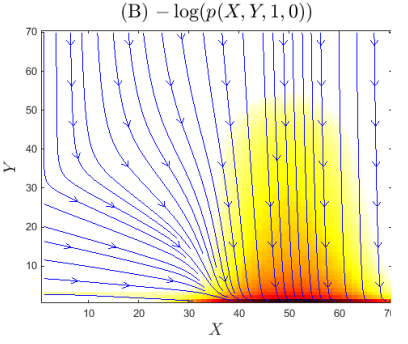

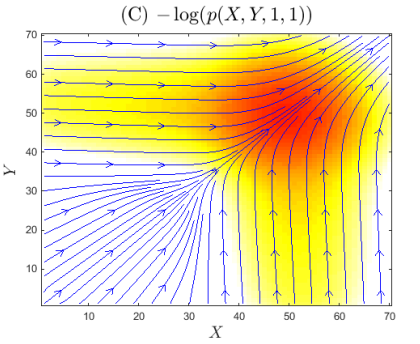

Liouville flux

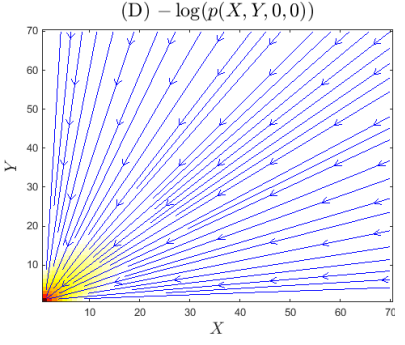

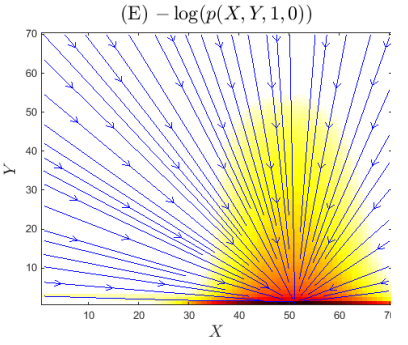

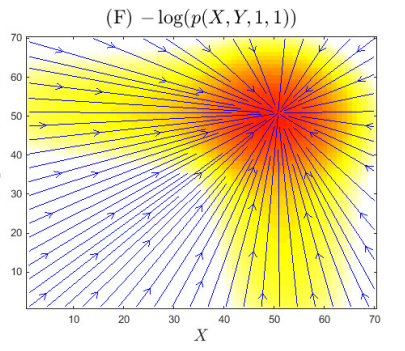

Fokker-Planck flux

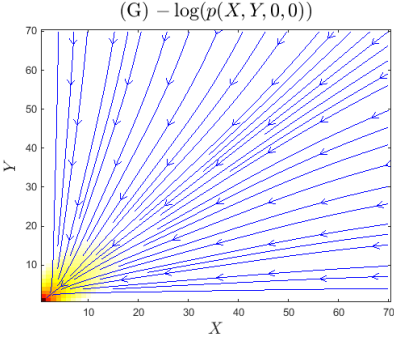

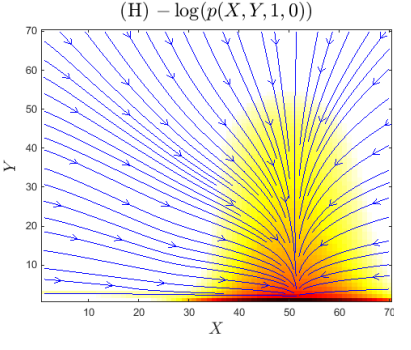

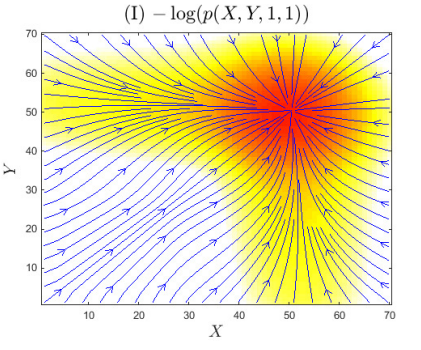

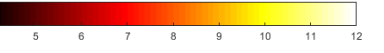

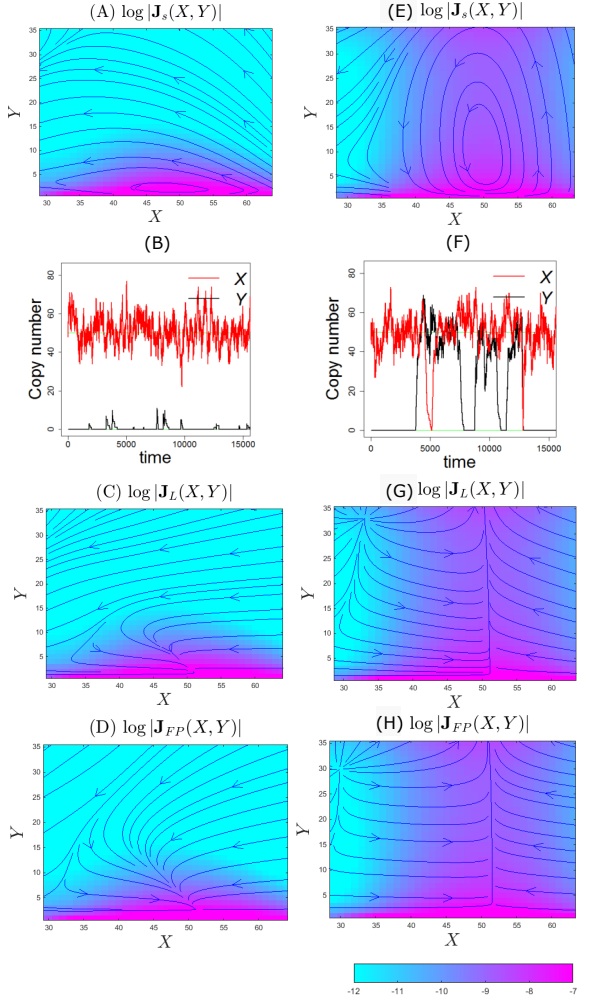
(A) $\log|\mathbf{J}_s(X,Y)|$
(E) $\log|\mathbf{J}_s(X,Y)|$
(B)
(F)
X
Y
Copy number
time
(C) $\log|\mathbf{J}_L(X,Y)|$
(G) $\log|\mathbf{J}_L(X,Y)|$
(D) $\log|\mathbf{J}_{FP}(X,Y)|$
(H) $\log|\mathbf{J}_{FP}(X,Y)|$
-12
-11
-10
-9
-8
-7